The RealGas and RealGasH2O Options of the TOUGH+ Code for the Simulation of Coupled Fluid and Heat Flow in Tight/Shale Gas Systems

George J. Moridis[1]* and Craig M. Freeman[2]

[1]Earth Sciences Division, Lawrence Berkeley National Laboratory
[2]Petroleum Engineering Dept., Texas A&M University

*Corresponding author. *Email address*:
GJMoridis@lbl.gov

Accepted for publication in October 2013 in the journal *Computers & Geosciences*

Available at:

http://dx.doi.org/10.1016/j.cageo.2013.09.010

Citation:

George J. Moridis, Craig M. Freeman, The RealGas and RealGasH2O Options of the TOUGH+ Code for the Simulation of Coupled Fluid and Heat Flow in Tight/Shale Gas Systems, *Computers & Geosciences*, http://dx.doi.org/10.1016/j.cageo.2013.09.010

The RealGas and RealGasH2O Options of the TOUGH+ Code for the Simulation Of Coupled Fluid And Heat Flow in Tight/Shale Gas Systems

George J. Moridis (a), and Craig M. Freeman (b)

[a]: Earth Sciences Division, Lawrence Berkeley National Laboratory

[b]: Petroleum Engineering Dept., Texas A&M University

Abstract

We developed two new EOS additions to the TOUGH+ family of codes, the `RealGasH2O` and `RealGas`. The `RealGasH2O` EOS option describes the non-isothermal two-phase flow of water and a real gas mixture in gas reservoirs, with a particular focus in ultra-tight (such as tight-sand and shale gas) reservoirs. The gas mixture is treated as either a single-pseudo-component having a fixed composition, or as a multicomponent system composed of up to 9 individual real gases. The `RealGas` option has the same general capabilities, but does not include water, thus describing a single-phase, dry-gas system. In addition to the standard capabilities of all members of the TOUGH+ family of codes (fully-implicit, compositional simulators using both structured and unstructured grids), the capabilities of the two codes include: coupled flow and thermal effects in porous and/or fractured media, real gas behavior, inertial

(Klinkenberg) effects, full micro-flow treatment, Darcy and non-Darcy flow through the matrix and fractures of fractured media, single- and multi-component gas sorption onto the grains of the porous media following several isotherm options, discrete and fracture representation, complex matrix-fracture relationships, and porosity-permeability dependence on pressure changes. The two options allow the study of flow and transport of fluids and heat over a wide range of time frames and spatial scales not only in gas reservoirs, but also in problems of geologic storage of greenhouse gas mixtures, and of geothermal reservoirs with multi-component condensable (H_2O and CH_4) and non-condensable gas mixtures.

The codes are verified against available analytical and semi-analytical solutions. Their capabilities are demonstrated in a series of problems of increasing complexity, ranging from isothermal flow in simpler 1D and 2D conventional gas reservoirs, to non-isothermal gas flow in 3D fractured shale gas reservoirs involving 4 types of fractures, micro-flow, non-Darcy flow and gas composition changes during production.

Keywords: numerical simulation, fractured media, multicomponent flow, coupled flow and heat flow, shale gas, real gas mixture

1. Introduction

1.1. Background

The ever-increasing energy demand, coupled with the advent and advances in reservoir stimulation technologies, has prompted an explosive growth in the development of unconventional gas resources in the U.S. during the last decade. Tight-sand and shale gas reservoirs are currently the main unconventional resources, upon which the bulk of production activity is currently concentrating (Warlick, 2006). Production from such resources in the U.S. has skyrocketed from virtually nil at the beginning of 2000, to 6%

of the gas produced in 2005 (U.S. EIA, 2007), to 23% in 2010, and is expected to reach 49% by 2035 (U.S. EIA, 2012). Production of shale gas is expected to increase from a 2007 U.S. total of 1.4 TCF to 4.8 TCF in 2020 (API, 2013). The ability to recover natural gas from shale gas formations has led to a dramatic increase in the estimate of the U.S. gas reserves, which increased by 35% from 2006 to 2008 (Mowad, 2009) and stood at 2000 TCF in 2009 (US DOE, 2009). In its Annual Energy Outlook for 2011, the US Energy Information Administration (EIA) more than doubled its estimate of technically recoverable shale gas reserves in the US from 353 TCF to 827 TCF by including data from recent drilling results in the Marcellus, Haynesville, and Eagle Ford shales (US EIA, 2011). Note that the bulk of the gas production from tight sands and shales has concentrated almost exclusively in North America (U.S. and Canada), and serious production elsewhere in the rest world has yet to begin. This leads to justified expectations that gas production from such ultra-tight systems may be one of the main sources (if not the main) source of natural gas in the world for decades to come, with 4 obvious implications and benefits for national economies and national energy security.

The importance of tight-sand and shale reservoirs as energy resources necessitates the ability to accurately estimate reserves and to evaluate, design, manage and predict production from such systems over a wide range of time frames and spatial scales. Modeling and simulation play a key role in providing the necessary tools for these activities. However, these reservoirs present challenges that cannot easily (if at all) handled by conventional gas models and simulators: they are characterized by extremely low permeabilities (often in the nD = 10^{-21} m^2 range), have native fractures that interact with the fractures created during the reservoir stimulation and with the matrix to result in

very complicated flow regimes and patterns that very often do not follow Darcy's Law, have pores of such small dimensions that interfere with the Brownian motion of the gas molecules (thus rendering standard advection-diffusion approaches irrelevant, and requiring accounting for Knudsen diffusion and special formulations of multi-component diffusion), exhibit highly non-linear behavior, have large amounts of gas sorbed onto the grains of the porous media in addition to gas stored in the pores, and may exhibit unpredictable geomechanical behavior such as the evolution of secondary fractures (Kim and Moridis, 2013) that may further complicate an already complex flow regime.

Several analytical models have been proposed to predict flow performance, and numerical studies have been conducted to analyze production from these ultra-tight reservoirs. Most of these studies have assumed idealized and regular fracture geometries, and include significant simplifying assumptions. Among the various analytical and semi-analytical solutions that have been proposed to model flow in shale-gas and tight-gas reservoirs, the early work of Gringarten (1971) and Gringarten et al. (1974) described the simplified flow through domains involving a single vertical fracture and a single horizontal fracture. More accurate semi-analytical models for single vertical fractures were developed later (e.g., Blasingame and Poe Jr., 1993). Prior to the development of models for multiply-fractured horizontal wells (Medeiros et al., 2006), it was common practice to represent these multiple fractures with an equivalent single fracture. More recently, several other analytical and semi-analytical models have been developed (Bello and Wattenbarger, 2008); Mattar, 2008; Anderson et al., 2010), but these, despite their 1 speed, cannot accurately handle the very highly nonlinear aspects of shale-gas and tight-gas reservoirs, cannot describe complex domain geometries, and cannot accurately

capture gas sorption and desorption from the matrix (a non-linear process that does not lend itself to analytical solutions), multiphase flow, unconsolidation, and several non-ideal and complex fracture networks (Houze et al., 2010).

The importance of such ultra-tight reservoirs and the shortcomings of the analytical and semi-analytical models have led to the development of numerical reservoir simulators that address the particularities of these systems. Miller et al., (2010) and Jayakumar et al., (2011) used numerical simulation to history-match and forecast production from two different shale-gas fields. Cipolla et al., (2009), Freeman (2010), Moridis et al., (2010) and Freeman et al., (2009; 2013) and conducted numerical sensitivity studies to identify the most important mechanisms and factors that affect shale-gas reservoir performance. Powerful commercial simulators with specialized options for shale gas analysis such as GEM (CMG, 2013) and ECLIPSE For Unconventionals (SLB, 2013) have become available. While these address the most common features of unconventional and ultra-tight media, they are designed primarily for large-scale production evaluation at the reservoir level and cannot be easily used for scientific investigations of micro-scale processes and phenomena in the vicinity of fractures.

1.2. The TOUGH+ Family of Codes

TOUGH+ is a family of public domain codes developed at the Lawrence Berkeley National Laboratory (Moridis et al., 2008) that are a successor to the TOUGH2 (Pruess et al., 1991) family of codes for multi-component, multiphase fluid and heat flow. It is written in standard FORTRAN 95/2003 to take advantage of all the object-oriented

capabilities and the enhanced computational features of that language. It employs dynamic memory allocation, follows the tenets of Object-Oriented Programming (OOP), and involves entirely new data structures and derived data types that describe the objects upon which the code is based. The TOUGH+ code is based on a modular structure that is designed for maximum traceability and ease of expansion.

TOUGH+ is a family of codes developed at the Lawrence Berkeley National Laboratory (Moridis et al., 2008) that are a successor to the TOUGH2 (Pruess et al., 1991) family of codes for multi-component, multiphase fluid and heat flow. It is written in standard FORTRAN 95/2003 to take advantage of all the object-oriented capabilities and the enhanced computational features of that language. It employs dynamic memory allocation, follows the tenets of Object-Oriented Programming (OOP), and involves entirely new data structures and derived data types that describe the objects upon which the code is based. The TOUGH+ code is based on a modular structure that is designed for maximum traceability and ease of expansion.

1.3. Objectives and Features

The main objective of this study was to develop numerical capabilities allowing the description of a wide range of processes involved in the non-isothermal flow through the spectrum of natural gas reservoirs in geologic systems, including tight-gas and shale-gas reservoirs with natural and/or induced fractures. A particular focus is the incorporation of capabilities to describe process and phenomena occurring during the non-isothermal flow of real gases in fractured ultra-tight reservoirs, including non-Darcy flow, Knudsen and multi-component diffusion, and interactions of rock matrix with both discrete fractures

with generalized fracture effect concepts such as dual- and multi-porosity (Warren and Root, 1963), dual-permeability, and multiple interactive continua (Pruess, 1983).

To that end, we developed two new EOS additions to the TOUGH+ family of codes: the `RealGasH2O` and `RealGas` options (hereafter referred to as T+GW and T+G, respectively) for the description of two-phase (aqueous and gas) and single-phase (dry-gas) flow through complex geologic media, respectively. The T+GW and T+G codes account for practically all known processes and phenomena, involve a minimum of assumptions, and are suitable for scientific investigations at any spatial (from the sub-mm scale in the vicinity of the fracture surface to the reservoir scale) and temporal scales, thus allowing insights into the system performance and behavior during production.

In addition to all the standard capabilities common to the TOUGH2 (Pruess et al., 1999) and TOUGH+ (Moridis et al. 2008) family of codes, the physics and thermodynamics of mass and heat flow through porous media in these two options include the most recent developments in the fields, and account for practically all known processes. The new capabilities can provide solutions to the problem of prediction of gas production from the entire spectrum of gas-bearing reservoirs, but also of any reservoir involving water and gas mixtures of up to nine components. Of particular interest are applications to ultra-tight reservoirs (including tight-sand and shale reservoirs), the numerical simulation of which may involve unstructured grids, extremely fine domain discretization, complex fracture-matrix interactions in several subdomains of the producing system, Darcy and non-Darcy flow, single- and multi-component sorption following a variety of isotherm options, and coupled thermophysical phenomena and processes.

Although this paper focuses mainly on problems of hydrocarbon gas flow through tight reservoirs, it is important to indicate that the T+GW code is fully applicable to a wide variety of other problems, including the study of the geological storage of greenhouse gas mixtures, and of geothermal reservoirs with multi-component non-condensable gas mixtures.

2. Code Description

The ensuing discussion focuses on the description of the T+GW code describing the two-phase flow problem of an aqueous and a gas phase flow through a geologic system. The T+G code is entirely analogous, differing only in the omission of water as a mass component, thus solving the much simpler problem of single-phase, dry-gas flow and production.

2.1. Fundamental Equations of Mass and Energy Balance

A non-isothermal fractured tight-gas or shale-gas system can be fully described by the appropriate mass balance equations and an energy balance equation. The following components κ, corresponding to the number of equations, are considered: $\kappa = g^i$, i.e., the various gaseous components (compounds) i constituting the natural gas ($i = 1, \ldots, N_G$, $N_G \geq 1$); water (w), and heat (θ), treated as a pseudo-component. The following nine gaseous components are currently available to T+GW and T+G: CH_4, C_2H_6, C_3H_8, C_4H_{10}, CO_2, H_2S, O_2, N_2 and H_2, all of which except CO_2 are treated as non-condensable. Note that in T+GW it is possible to treat a real gas mixture of constant composition (i.e., with non-variant mole fractions Y^i) as a *single pseudo-component*, the properties of which vary with the pressure P and temperature T.

Following Pruess et al. (1999), mass and heat balance considerations in every subdomain (gridblock) into which the simulation domain is been subdivided by the integral finite difference method in TOUGH+ dictates that

$$\frac{d}{dt}\int_{V_n} M^\kappa dV = \int_{\Gamma_n} \mathbf{F}^\kappa \cdot \mathbf{n}\, dt + \int_{V_n} q^\kappa dV \quad \text{.....(1)}$$

where V, V_n are the volume and volume of subdomain n [m^3]; M^κ is the mass accumulation term of component κ [kg m^{-3}]; A and Γ_n are the surface area and surface of subdomain n [m^2], respectively; $\mathbf{F}^\kappa$ is the flow vector of component κ [kg $m^{-2}s^{-1}$]; **n** is the inward unit normal vector; q^κ is the source/sink term of component κ [kg $m^{-3}s^{-1}$]; and t is the time [s].

2.1.1.Mass accumulation terms. Under the two-phase (aqueous and gas) flow conditions described by T+GW, the mass accumulation terms M^k for the mass components κ in equation (1) are given by

$$\sum_{\beta \equiv A,G} \phi\, S_\beta \rho_\beta X_\beta^\kappa + \delta_\Psi (1-\phi)\rho_R \Psi^i \quad \text{.....(2)}$$

where $\kappa \equiv w, g^i$, $i = 1, ..., N_G$; ϕ is the porosity [*dimensionless*]; ρ_β is the density of phase β [kg m^{-3}]; S_β is the saturation of phase β [*dimensionless*]; X_β^κ is the mass fraction of component in phase β [kg/kg]; ρ_R is the rock density [kg m^{-3}]; Ψ^i is the mass of sorbed component g^i per unit mass of rock [kg/kg]; and $\delta_\Psi = 0$ for non-sorbing media (including tight-gas systems) that are usually devoid of substantial organic carbon, while $\delta_\Psi = 1$ in gas-sorbing media such as shales.

The first term in equation (2) describes fluid mass stored in the pores, and the second the mass of gaseous components sorbed onto the organic carbon (mainly kerogen)

content of the matrix of the porous medium. The latter is quite common in shales. Although gas desorption from kerogen has been studied extensively in coalbed CH_4 reservoirs, and several analytic/semi-analytic models have been developed for such reservoirs (Clarkson and Bustin, 1999), the sorptive properties of shale are not necessarily analogous to coal (Schettler and Parmely, 1991).

2.1.2. Gas sorption terms. The most commonly used empirical model describing sorption onto organic carbon in shales is analogous to that used in coalbed methane and follows the Langmuir isotherm that, for a single-component gas, is described by

$$\begin{cases} \Psi^i = \dfrac{p_{dG} m_L}{p_{dG} + p_L} & \text{for ELaS} \\ \dfrac{d\Psi^i}{dt} = k_L \left(\dfrac{p_{dG} m_L}{p_{dG} + p_L} - \Psi^i \right) & \text{for KLaS} \end{cases} \quad \text{..... (3)}$$

where p_{dG} is the dry gas pressure ($p_{dG} = p_G - p^v$, where p^v is the partial pressure of the water vapor), ELaS indicates Equilibrium Langmuir Sorption, and KLaS denotes Kinetic Langmuir Sorption. The m_L term in equation (3) describes the total mass storage of component g^i at infinite pressure (kg of gas/kg of matrix material), p_L is the pressure at which half of this mass is stored (Pa), and k_L is a kinetic constant of the Langmuir sorption (1/s). In most studies applications, an *instantaneous equilibrium* is assumed to exist between the sorbed and the free gas, i.e., there is no transient lag between pressure changes and the corresponding sorption/desorption responses and the equilibrium model of Langmuir sorption is assumed to be valid. Although this appears to be a good approximation in shales (Gao et al., 1994) because of the very low permeability of the matrix (onto which the various gas components are sorbed), the subject has not been fully investigated. For multi-component gas, equation (3) becomes

$$\begin{cases} \Psi^i = \dfrac{p_{dG} B^i m^i{}_L \Upsilon^i}{1 + p_{dG} \sum_i B^i \Upsilon^i} & \text{for ELaS} \\ \dfrac{d\Psi^i}{dt} = k_L^i \left(\dfrac{p_{dG} B^i m^i{}_L \Upsilon^i}{1 + p_{dG} \sum_i B^i \Upsilon^i} - \Psi^i \right) & \text{for KLaS} \end{cases} \quad \text{..... (4)}$$

where B^i is the Langmuir constant of component g^i in 1/Pa (Pan et al., 2008), and Y^i is the dimensionless mole fraction of the gas component i in the water-free gas phase. Note that the T+GW and T+G codes offer the additional options of linear and Freundlich sorption isotherms (equilibrium and kinetic). For each gas component g^i, these are described by the following equations:

$$\begin{cases} \Psi^i = K_l^i \, p^i & \text{for ELiS} \\ \dfrac{d\Psi^i}{dt} = k_l^i \left(K_l^i \, p^i - \Psi^i \right) & \text{for KLiS} \end{cases} \quad \text{..... (5)}$$

$$\begin{cases} \Psi^i = K_F^i \, \left(p^i \right)^c & \text{for EFS} \\ \dfrac{d\Psi^i}{dt} = k_F^i \left[K_F^i \, \left(p^i \right)^c - \Psi^i \right] & \text{for KFS} \end{cases} \quad \text{..... (6)}$$

where ELiS and KLiS denote equilibrium and kinetic linear sorption, respectively; EFS and KFS denote equilibrium and kinetic Freundlich sorption, respectively; K^i_l and K^i_F are the distribution coefficients of the ELiS and EFS sorption isotherms of gas component i, respectively; p^i is the partial pressure of g^i; k^i_l and k^i_F are the kinetic coefficients of the ELiS and EFS sorption isotherms of g^i, respectively; and c is the exponent of the Freundlich sorption isotherm.

2.1.3. Heat accumulation terms. The heat accumulation term includes contributions from the rock matrix and all the phases, and is given by the equation

$$M^{\theta} = \begin{cases} (1-\phi)\rho_R \int_{Tr}^{T} C_R(T)\, dT + \\ \sum_{\beta=A,G} \phi S_\beta \rho_\beta U_\beta + \delta_\Psi (1-\phi)\rho_R \sum_{i=1}^{N_G} u^i \Psi^i \end{cases} \quad \text{.....(7)}$$

where $C_R = C_R(T)$ is the heat capacity of the dry rock [J kg^{-1} K^{-1}]; U_β is the specific internal energy of phase β [J kg^{-1}]; $(u^i)_*$ is the specific internal energy of sorbed gas component g^i , including departure effects [J kg^{-1}]; T is the temperature [K]; and T_r is a reference temperature [K]. The specific internal energy of the gaseous phase is a very strong function of composition, is related to the specific enthalpy of the gas phase H_G, and is given by

$$U_G = \sum_{\kappa=w,g^i(i=1,N_G)} X_G^\kappa\, u^\kappa + U_{dep} \quad \left(= H_G - \frac{P}{\rho_G} \right) \quad \text{.....(8)}$$

where u^κ is the specific internal energy of component κ in the gaseous phase, and U_{dep} is the specific internal energy departure of the gas mixture [J kg^{-1}]. The internal energy of the aqueous phase accounts for the effects of gas and inhibitor solution, and is estimated from

$$U_A = X_A^w u^w + \sum_{i=1}^{N_G} X_A^{g^i} \left(u^i + U_{sol}^i \right) \quad \text{..... (9)}$$

where u^w and u^i are the ideal parts of the specific internal energies of H_2O and of natural gas component g^i at the p and T conditions of the aqueous phase, respectively, and U^i_{sol} are the specific internal energies of dissolution of the gas component g^i in H_2O (obtained from tables). Note that the reference state for all internal energy and enthalpy computations are p = 101300 Pa and T = 273.15 K (0 ^{o}C).

2.1.4. Fluid flux terms. The mass fluxes of water and of the gaseous components include contributions from the aqueous and gaseous phases, i.e.,

$$\mathbf{F}^{\kappa} = \sum_{\beta \equiv A,G} \mathbf{F}_{\beta}^{\kappa},\ \kappa \equiv w, g^{i},\ i = 1,...,N_G \quad \text{..... (10)}$$

For phase β, $\mathbf{F}_{\beta}^{\kappa} = X_{\beta}^{\kappa}\mathbf{F}_{\beta}$. In T+GW and T+G, there are three options to describe the phase flux $\mathbf{F}_{\beta}$. The first is the standard Darcy's law, i.e.,

$$\mathbf{F}_{\beta} = \rho_{\beta}\left[-\frac{k\ k_{r\beta}}{\mu_{\beta}}\nabla\Phi_{\beta}\right] = \rho_{\beta}\mathbf{v}_{\beta},\quad \nabla\Phi_{\beta} = \nabla p_{\beta} - \rho_{\beta}\mathbf{g}, \text{...(11)}$$

where k is the rock intrinsic permeability [m^2]; $k_{r\beta}$ is the relative permeability of phase β [dimensionless]; μ_{β} is the viscosity of phase β [Pa s]; p_{β} is the pressure of phase β [Pa]; and **g** is the gravitational acceleration vector [m s^{-2}]. In T+GW, the relationship between the aqueous and the gas pressures, p_A and p_G, respectively, is given by $p_A = p_G + P_{cGA}$, where P_{cGA} is the gas-water capillary pressure [Pa]. The $k_{r\beta}$ and P_{cGA} options are the standard ones available in the TOUGH2 and TOUGH+ family of codes (Pruess et al., 1999; Moridis et al., 2008).

The mass flux of component κ in the gas phase incorporates advection and diffusion contributions, and is given by

$$\mathbf{F}_{G}^{\kappa} = \left(1 + \frac{b}{P_G}\right)\rho_G \mathbf{v}_G X_G^{\kappa} - \underbrace{\phi S_G \tau_G D_G^{\kappa}}_{-\mathbf{J}_G^{\kappa}}\underline{\rho_G \nabla X_G^{\kappa}}, \text{ ..... (12)}$$

where b is the *Klinkenberg* (1941) b-factor accounting for gas slippage effects [Pa], the term $\mathbf{J}_G^{\kappa}$ is the diffusive mass flux of component κ in the gas phase [kg m^{-2} s^{-1}], D_G^{κ} is the multicomponent molecular diffusion coefficient of component κ in the gas phase in the absence of a porous medium [m^2 s^{-1}], and τ_G is the gas tortuosity [dimensionless].

The Klinkenberg *b*-factor is either provided as input, or is computed using the relationship proposed by Jones (1972) as

$$\frac{b}{b_r} = \left(\frac{k}{k_r} \right)^{-0.36}, \quad \text{..... (13)}$$

where the subscript *r* denotes a reference medium with a known *b*-factor and *k*, such as those listed by Wu et al. (1998). There are several methods to compute τ_G in the T+GW and T+G codes, including the Millington and Quirk (1961) model.

The diffusive mass fluxes of the water vapor and the natural gas components are related through the relationship of Bird et al. (2007)

$$\mathbf{J}_G^w + \sum_{i=1}^{N_G} \mathbf{J}_G^{g^i} = 0, \quad \text{..... (14)}$$

which ensures that the total diffusive mass flux of the gas phase is zero with respect to the mass average velocity when summed over the components. Then the total mass flux of the gas phase is the product of its velocity and density.

If the flow is non-Darcian, then the equation $\mathbf{F}_\beta = \rho_\beta \mathbf{v}_\beta$ still applies, but $\mathbf{v}_\beta$ is now computed from the solution of the quadratic equation

$$\nabla \Phi_\beta = -\left(\frac{\mu_\beta}{k\, k_{r\beta}} \mathbf{v}_\beta + \beta_\beta \rho_\beta \mathbf{v}_\beta \left| \mathbf{v}_\beta \right| \right), \quad \text{..... (15)}$$

in which β_β is the "turbulence correction factor" (Katz et al., 1959). The quadratic equation in (14) is the general momentum-balance *Forcheimer equation* (Forchheimer, 1901; Wattenbarger and Ramey, 1968), and incorporates laminar, inertial and turbulent effects. This is the second option. The solution then is

$$\mathbf{v}_\beta = \frac{2\nabla\Phi_\beta}{\frac{\mu_\beta}{k\ k_{r\beta}} + \sqrt{\left(\frac{\mu_\beta}{k\ k_{r\beta}}\right)^2 + 4\beta_\beta\rho\left|\nabla\Phi_\beta\right|}}, \quad \text{..... (16)}$$

and $\mathbf{v}_\beta$ from equation (15) is then used in the equations of flow (11) and (12). T+GW and T+G offer 13 options to compute β_β, several of which are listed in Finsterle (2001). The third option follows the approach of Barree and Conway (2007), as described by Wu et al. (2011), which involves a different formulation of $\nabla\Phi_\beta$.

2.1.5. Heat flux terms. The heat flux accounts for conduction, advection and radiative heat transfer, and is given by

$$\mathbf{F}^\theta = -\bar{k}_\theta\nabla T + f_\sigma\sigma_0\nabla T^4 + \sum_{\beta\equiv A,G} H_\beta\mathbf{F}_\beta \text{ , ...(17)}$$

where $\bar{k}_\theta$ is a representative thermal conductivity of the reservoir fluids-impregnated rock [W m^{-1} K^{-1}]; h_β is a specific enthalpy of phase β [J kg^{-1}]; f_σ is the radiance emittance factor [dimensionless]; σ_0 is the Stefan-Boltzmann constant [5.6687×10^{-8} J m^{-2} K^{-4}]. The specific enthalpy of the gas phase is computed as

$$H_G = \sum_{\kappa\equiv w,g_i} X_G^\kappa h_G^\kappa + H_{dep} \text{ ,.....(18)}$$

where h_G^κ is the specific enthalpy of component κ in the gaseous phase, and H_{dep} is the specific enthalpy departure of the gas mixture [J kg^{-1}]. The specific enthalpy of the aqueous phase is estimated from

$$H_A = X_A^w h_A^w + \sum_i X_A^{g^i}\left(h_A^{g^i} + H_{sol}^{g^i}\right), \text{ ……..... (19)}$$

where h_A^w and $h_A^{g^i}$ are the specific enthalpies of H_2O and of the natural gas components in the aqueous phase, respectively, and $H_{sol}^{g^i}$ is the specific enthalpy of dissolution [J kg^{-1}] of gas component g^i in the aqueous phase.

2.1.5. Source and sink terms. In sinks with specified mass production rate, withdrawal of the mass component κ is described by

$$q^\kappa = \sum_{\beta \equiv A,G} X_\beta^\kappa q_\beta, \quad \kappa = w, g^i \ (i = 1, ..., N_G), \ldots\ldots (20)$$

where q_β is the production rate of the phase β [kg m^{-3}]. For a prescribed production rate, the phase flow rate q_β is determined from the phase mobility at the location of the sink. For source terms (well injection), the addition of a mass component κ occurs at desired rates. The contribution of the injected or produced fluids to the heat balance of the system are described by

$$q^\theta = \sum_{\beta = A,G} q_\beta H_\beta, \ldots\ldots\ldots\ldots\ldots\ldots (21)$$

where q^θ is the rate of heat addition or withdrawal in the course of injection or production, respectively (W/kg).

2.1.6. P- and T-dependence of ϕ and k. The effect of pressure change on the porosity of the matrix is described by two options. The first involves the standard exponential equation

$$\phi = \phi_r \exp\left[\alpha_p \left(p - p_r\right) + \alpha_T \left(T - T_r\right)\right], \ldots\ldots\ldots\ldots (22)$$

where α_T is the thermal expansivity of the porous medium (1/K) and α_p is the pore compressibility (1/Pa), which can be either a fixed number or a function of pressure (Moridis et al., 2008). A second option describes the *p*-dependence of ϕ as a polynomial

function of p. The ϕ - k relationship is described by the general expression of Rutqvist and Tsang (2003) as:

$$\frac{k}{k_r} = exp\left[\gamma\left(\frac{\phi}{\phi_r} - 1\right)\right], \quad \text{.....(23)}$$

where γ is an empirical permeability reduction factor that ranges between 5 (for soft unconsolidated media) and 29 (for lithified, highly consolidated media). Note that the equations described here are rather simple and apply to matrix ϕ and k changes when the changes in p and T are relatively small. These equations are not applicable when large pressure and temperature changes occur in the matrix, cannot describe the creation of new (secondary) fractures and cannot describe the evolution of the characteristics of primary and secondary fractures (e.g., aperture, permeability, extent, surface area) over time as the fluid pressures, the temperatures, the fluid saturations and the stresses change. For such problems, it is necessary to use the T+M model (Kim and Moridis, 2013) that couples the flow-and-thermal-process T+RW simulator discussed here with the ROCMECH geomechanical code. This coupled model accounts for the effect of changing fluid pressures, saturations, stresses, and temperatures on the geomechanical regime and provides an accurate description of the evolution of ϕ and k over the entire spectrum of p and T covered during the simulation.

2.2. Physical – Chemical Processes

2.2.1.Micro-flow: Knudsen diffusion and Dusty Gas model. For ultra-low permeability media (such as tight sands and shales) and the resulting micro-flow processes, the Klinkenberg b-factor for a single- component or pseudo-component gas in

T+GW and T+G is computed by the method of Florence et al. (2007) and Freeman et al. (2011) as

$$\frac{b}{P_G} = \left(1+\alpha_K K_n\right)\left(1+\frac{4K_n}{1+K_n}\right)-1, \quad \text{..... (24)}$$

where K_n is the Knudsen diffusion number (dimensionless), which characterizes the deviation from continuum flow, accounts for the effects of the mean free path of gas molecules $\bar{\lambda}$ being on the same order as the pore dimensions of the porous media, and is computed from (Freeman et al., 2011) as

$$K_n = \frac{\bar{\lambda}}{r_{pore}} = \frac{\mu_G}{2.81708 p_G}\sqrt{\frac{\pi RT}{2M}\frac{\phi}{k}}, \quad \text{..... (25)}$$

with M being the molecular weight and T the temperature (K). The term a_K in Eq. 24 is determined from Karniadakis and Beskok (2001) as

$$\alpha_K = \frac{128}{15\pi^2}\tan^{-1}\left(4K_n^{0.4}\right), \quad \text{..... (26)}$$

For simplicity, we have omitted the *i* superscript in equations (23) to (26). The Knudsen diffusion can be very important in porous media with very small pores (on the order of a few micrometers or smaller) and at low pressures. For a single gas pseudo-component, the properties in (26) are obtained from an appropriate equation of state for a real-gas mixture of constant composition Y^i. The Knudsen diffusivity D_K [m^2/s] can be computed as (Civan, 2008; Freeman et al., 2011)

$$D_K = \frac{4\sqrt{k\phi}}{2.81708}\sqrt{\frac{\pi RT}{2M}} \quad \text{or} \quad D_K = \frac{kb}{\mu_G} \quad \text{..... (27)}$$

For a multicomponent gas mixture that is not treated as a single pseudo-component, ordinary Fickian diffusion must be taken into account as well as Knudsen diffusion**.** Use

of the advective–diffusive flow model (Fick's law) should be restricted to media with $k \geq 10^{-12}$ m^2; the dusty-gas model (DGM) is more accurate at lower k (Webb and Pruess, 2003). Additionally, DGM accounts for molecular interactions with the pore walls in the form of Knudsen diffusion. Shales may exhibit a permeability k as low as 10^{-21} m^2, so the DGM described below is more appropriate than the Fickian model (Webb and Pruess, 2003; Doronin and Larkin 2004; Freeman et al., 2011):

$$\sum_{j=1, j\neq i}^{N_G} \frac{Y^i N_D^j - Y^j N_D^i}{D_e^{ij}} - \frac{N_D^i}{D_K^i} = \frac{p^i \nabla Y^i}{ZRT} + \left(1 + \frac{kp}{\mu_G D_K^i}\right) \frac{Y^i \nabla p^i}{ZRT} \quad \text{..... (28)}$$

where N^i_D is the molar flux of component g^i [mole m^{-2}s^{-1}], D_e^{ij} is the effective gas (binary) diffusivity of species g^i in species g^j, and $D_K{}^i$ is the Knudsen diffusivity of species g^i.

2.2.2. Gas solubility

There are two options for estimating the solubility of a gas i into the aqueous phase in T+GW. The first (and simpler one) is based on Henry's Law, described by the relationship

$$p^i = H^i X_A^i, \quad \text{..... (29)}$$

where H^i [Pa] a T-dependent, species-specific factor referred to as Henry's factor (as opposed to its customary name as Henry's *constant*). T+GW includes a library of fast parametric relationships of $H^i = H^i(\mathrm{T})$ that cover a wide range of T and are applicable over a wide range of p, and this is the preferred option if a single gas component or pseudo-component is involved. The second option is based on the equality of fugacities in the aqueous and the gas phase, involves the chemical potentials of the various species in solution, and is applicable when p is very high, when there is significant dissolved

species interaction and/or dissolved salts (not the case in T+RW, which does include an equation for salts).

2.2.3. Thermophysical properties

The water properties in the T+GW code are obtained from steam table equations (IFC, 1967), as implemented in other members of the TOUGH family of codes (Pruess et al., 1999; Moridis et al., 2008), and cover a wide pressure and temperature range (from 10^{-4} MPa to 10^{3} MPa, and from 235K to 1273K).

All the real gas properties in T+G and T+GW are computed from one of the three available options of cubic equations of state (EOS) - i.e., the Peng-Robinson (1973), the Redlich-Kwong (1949) and the Soave-Redlich-Kwong (1973) EOS- that were implemented by Moridis et al. (2008). The gas property package computes the compressibility, density, fugacity, specific enthalpy and internal energy (ideal and departure) of pure gases and gas mixtures over a very wide range of pressure and temperature conditions. Additionally, the package uses the cubic equations of state to compute the gas viscosity and thermal conductivity using the method of Chung et al. (1988), and binary diffusivities from the method of Fuller et al. (1969) and Riazi and Whitson (1993). In addition to the standard cubic equation of state, the thermodynamics of the T+GW and T+G package include a complete phase diagram of CO_2 (from liquid to gas to supercritical gas, and the corresponding thermophysical properties) that is based on a modification of the approach in the ECO2M package (Pruess, 2011) of TOUGH2 (Pruess et al., 1999).

3. The Solution Approach

Following the standard approach in the TOUGH Prues et al., 1999) and TOUGH+ (Moridis et al., 2008) family of codes, the continuum equation (1) is discretized in space using the Integral Finite Difference (IFD) method (Edwards, 1972; Narasimhan and Witherspoon, 1976). The space discretization approach used in the IFD method and the definition of the geometric parameters are illustrated in Figure 1. Note that, as Figure 1 indicates, the IFD method is not limited to structured (regular) grids, but is directly applicable to any irregularly shaped subdomains (unstructured grid) m and n as long as the line D_{nm} connecting the centers of gravity between two gridblocks m and n is perpendicular to their common area A_{mn}.

Of particular importance to the description of flow through fractured media (as is invariably the case in tight reservoirs) in the T+G and T+GW codes is the availability of the method of Multiple Interacting Continua (MINC) (Pruess and Narasimhan, 1982; 1985; Pruess, 1983). This method allows the accurate description of coupled fluid and heat flows with steep gradients at the fracture-matrix interfaces by appropriate subgridding of the matrix blocks. The MINC concept is based on the notion that changes in fluid pressures, temperatures, and phase compositions due to the presence of sinks and sources (production and injection wells) will propagate rapidly through the fracture system, while invading the tight matrix blocks only slowly. Therefore, changes in matrix conditions will (locally) be controlled by the distance from the fractures. Fluid and heat flow from the fractures into the matrix blocks, or from the matrix blocks into the fractures, can then be modeled by means of one-dimensional strings of nested grid blocks.

The resulting discretized equations are expressed in residual form, are then linearized by the Newton-Raphson method and are solved fully implicitly. The resulting Jacobian is solved in the standard approach used in all TOUGH applications (Pruess et al., 1999). In T+G, the primary variables that constitute the solution vector are p_G, Y^i (i = 1,…, N_G), and T; in T+GW, the primary variables are the same for single-phase gas; p, X^i_A (i = 1,…, N_G) and T for single-phase aqueous conditions, and p_G, S_A, Y^i (i = 1,…, N_G-1) and T for two-phase conditions.

4. Validation and Verification Examples

We validated the T+G and T+GW codes by comparing them to the results of analytical solutions that covered the widest possible spectrum of the capabilities available in the codes. The analytical solutions included: the transient radial flow of a gas using pseudopressure (Fraim and Wattenbarger 1987); the pseudosteady-state radial flow of a slightly compressible liquid (Blasingame 1993; Dietz 1965); the Warren and Root solution for dual-porosity flow in a fractured reservoir (Warren and Root 1988; Pruess and Narasimhan 1982); the Wu analytical solution for Klinkenberg flow (Wu et al. 1988); and the Cinco-Meng solution for flow into a vertical fracture intercepting a well (Cinco-Ley and Meng 1988). The Peng-Robinson (1973) cubic equation of state (EOS) was used to evaluate the real gas properties in all validation and application problems.

4.1. Problem V1: Real gas transient flow in a cylindrical reservoir

Using the concept of pseudo-pressure, Fraim and Wattenbarger (1986) developed a solution to the problem of transient flow in a finite cylindrical real-gas reservoir with a producing vertical well at its center, described as:

$$p_D = \frac{1}{2} E_i \left(\frac{r_D^2}{4t_D} \right), \quad \text{.....(30)}$$

where E_i denotes the exponential integral,

$$p_D = \frac{kh}{q_V B \mu}(\psi_0 - \psi), \quad r_D = \frac{r}{r_w}, \quad t_D = \frac{k}{\phi \mu c_t r_w^2} t, \quad \psi = 2 \int_{p_r}^{p} \frac{p}{\mu z} dp,$$

.....(31)

ψ is the pseudo-pressure, r is the radius, r_w is the well radius [m], p is the pressure [Pa], p_r is a reference pressure [Pa], c_t is the total compressibility [Pa^{-1}], q_V is the volumetric production rate [ST m^3/s], B is the formation volume factor, and h is the reservoir thickness. The subscript *0* indicates initial conditions, and the subscript *D* denotes dimensionless variables.

The data used in the simulation of this validation problem appear in Table 1. The gas was 100% CH_4. The cylindrical domain discretization involved a single layer, and a total of 32 logarithmically increasing Δr's. Figure 2 shows a very good agreement of the analytical and the T+GW numerical solutions at various sampling times. The T+G code yields an identical solution. Note that the problem was solved both isothermally and non-isothermally, and the difference between the two solutions was very small and localized in the vicinity of the well. This difference is attributed to Joule-Thomson cooling effects because of the bigger pressure drops and the high gas velocity at this location.

4.2. Problem V2: Water flow in a cylindrical reservoir

Following from the work of Dietz (1965) in characterizing pressure buildup response, Blasingame (1993) developed a set of analytical solution of pseudo-steady state flow of a slightly compressible liquid in infinite and bounded circular reservoirs with a producing

well at their centers. For the case of a bounded aquifer with a well producing at a constant rate and with impermeable boundaries at $r=r_e$, the pressure distribution during a pseudo-steady-state regime is given by the following Blasingame (1993) solution:

$$p(r) = p_0 - \frac{qB\mu}{2\pi kh}\left(\ln\left(\frac{r_e}{r}\right) + \left(\frac{1}{2}\right)\frac{\left(r^2 - r_w^2\right)}{\left(r_e^2 - r_w^2\right)} + 0.75 \right) - \frac{qBt}{V_p c_t}, \ldots\ldots\ldots\ldots\ldots\ldots (32)$$

where V_p is the system pore volume (m^3).

The terms B, μ, c_t reflect water properties at the appropriate pressure and temperature. Using the data listed in Table 2, the T+GW solution in Figure 3 (based on the same grid with logarithmically increasing Δr's discussed in problem V1) practically coincides with the analytical solution.

4.3. Problem V3: The Warren and Root (1963) solution of flow in a dual porosity reservoir

Dual porosity flow occurs in fractured reservoirs where a network of high-permeability fractures is distributed throughout the low-permeability bulk matrix. In a particular conceptual construct, the matrix and the fracture network represent the two porosity systems and there is no flow between matrix blocks: flow occurs in the fractures, which are replenished by fluids from the matrix blocks. Warren and Root (1963) used the ratio of the permeabilities and storativities of the two porosity systems to mathematically describe the equations governing fluid flow as follows:

$$p_D\left(t_D, r_D, \omega, \lambda, s\right) = \frac{1}{2}\ln\left[\frac{4}{e^{\gamma}}\frac{t_D}{r_D^2}\right] - \frac{1}{2}E_1\left[\frac{\lambda}{\omega\left(1-\omega\right)}t_D\right] + \frac{1}{2}E_1\left[\frac{\lambda}{1-\omega}t_D\right] + s, \ldots (33)$$

where λ and α are the interporosity and the matrix block shape parameters, respectively, defined as

$$\lambda = \alpha r_w^2 \frac{k_m}{k_f} \quad \text{and} \quad \alpha = \frac{4n(n+2)}{l^2}, \quad \text{.....(34)}$$

where n is the number of normal sets of fractures (1,2 or 3), and l is the fracture spacing [m].

$V_{f,}$ is defined as the void fraction corresponding to the fraction of the reservoir occupied by the fractures. Generally the porosity of the fractures, ϕ_f, is assumed to equal 1, meaning that the fractures are open and do not contain any internal grain structure. The total volume fraction occupied by the fractures as a fraction of bulk volume is thus

$$f_f = \phi_f V_f \quad \text{..... (35)}$$

□□□□□□□ ω, the storativity ratio, is

$$\omega = \frac{\phi_f V_f c_f}{\left[\phi_f V_f c_f + \phi_m V_m c_m\right]}, \quad \text{.....(36)}$$

where the subscripts f and m denote fracture and matrix properties, respectively. The Warren and Root (1963) solution involves the following dimensionless variables:

$$p_D = p_{dc} \frac{k_f h}{qB\mu}(p_0 - p_r),\ t_D = t_{dc} \frac{k_f}{\mu(\phi_f V_f c_f + \phi_m V_m c_m) r_w^2} t,\ r_D = \frac{r}{r_w} \text{.....(37)}$$

A few extra parameters are defined for convenience, as the process of creating a MINC-based TOUGH mesh (Pruess et al., 2001) that reflects a given set of Warren and Root parameters involves some manipulation. The fracture aperture δ is defined through the equivalent continuum fracture porosity (Pruess and Narasimhan 1982) as

$$\delta = \frac{l\phi_{f,cont}}{3}, \quad \text{.....(38)}$$

The absolute (intrinsic) fracture permeability $k_{f,abs}$ is estimated from the relation

$$k_{f,abs} = \frac{\delta^2}{12}, \ldots\ldots\ldots\ldots\ldots\ldots\ldots\ldots\ldots\ldots\ldots\ldots (39)$$

and the adjusted fracture continuum permeability is computed from

$$k_{f,cont} = \frac{2k_{f,abs}\delta}{l}, \ldots\ldots\ldots\ldots\ldots\ldots\ldots\ldots\ldots\ldots\ldots\ldots (40)$$

Table 3 lists the various properties (reservoir and fluid) and parameters (reservoir dimensions and geometry) used in the analytical and numerical computations. Table 4 includes the fracture and matrix flow properties (porosity and permeability) used in the Warren and Root (1963) analytical solutions, in the MINC mesh generation and in the T+GW simulations. Note that the two cases that are investigated differ only in the fracture permeability. Table 5 lists the values of important parameters of the Warren and Root (1963) solution, as computed from the other inputs. The T+GW radial system mesh involved a single layer and 91 logarithmically-distributed elements in 2 MINC continua: fractures and matrix.

The comparisons between the analytical solutions and the numerical solutions in Cases 1 and 2 are shown in Figure 4. The agreement between the two solutions in both cases is good to very good.

4.4. Problem V4: Non-Darcy (Klinkenberg) gas flow

The Klinkenberg (1941) correction was originally developed to correct for the effect of gas slippage phenomena on permeability measurements of tight core samples. Depending on the flow rate, unconventional shale gas and tight gas sands may exhibit slip flow, or "Klinkenberg flow," in the reservoir itself. In order to correctly capture flow through such very low permeability media, the flow equations are derived in such a way

that permeability is treated as a function of pressure that deviates from the theoretical permeability at infinite gas pressure according to:

$$k_g = k_\infty \left(1 + \frac{b}{p} \right) \quad \text{..... (41)}$$

As discussed earlier, there are several options for the computation of the Klinkenberg parameter b, e.g., see Equation (16). Wu et al. (1988) used the pressure function $p_k = p + b$ to derived the following analytical solution to the problem of gas flow through an infinite cylindrical reservoir produced at a constant rate q:

$$p_k^2(r,t) = p_{k0}^2 - \frac{\mu q}{2\pi k_\infty h c_t} Ei\left(-\frac{k_\infty p_k r^2}{4\phi\mu t} \right) \quad \text{.....(42)}$$

The input parameters used in this problem are listed in Table 6. The gas was 100% CH_4. The cylindrical mesh used in the T+G and T+GW simulations involved a single layer and comprised 31 elements with logarithmically distributed Δr sizes. The agreement between the Wu at al. (1988) and the T+G solutions is excellent, as Figure 5 clearly indicates. The T+G and the T+GW solutions coincide. Additionally, given the short duration of the simulated period, the differences between the numerical predictions for isothermal and non-isothermal flow were practically negligible.

4.4. Problem V5: Flow into a vertical fracture with a well at its center

The solution of Cinco-Ley and Meng (1988) describes flow from a rectangular reservoir into a finite-conductivity vertical fracture intersected by a well at its center. The single bi-wing vertical fracture is a stimulation treatment typically applied to vertical wells in low-permeability reservoirs. This complicated model transitions between two

flow regimes over time. Bi-linear flow, where the dominant flow is through and perpendicular to the fracture face, is assumed at early times. At later times, the regime transitions into pseudo-radial flow.

The Cinco-Ley and Meng (1988) solution assumes flow for a slightly compressible liquid. In our computations, we used water as the reservoir fluid. The properties and conditions used in the computations of two cases (differing only in the fracture permeability) in this problem are listed in Table 7. The Cartesian domain in the T+GW study involved a single layer, and was discretized into 60x60x1 = 3400 elements in (x,y,z). The comparisons in Figure 6 between the analytical and the T+GW solutions in the two cases (involving different values of $F_{CD} = k_f b_f/(k_m x_f)$, as k_f was different) show a very good agreement.

5. Application Examples

The application examples include problems of increasing complexity, involving complex 3D domains, multiple fracture-matrix interactions, real gas mixtures composed of several components, and isothermal and non-isothermal systems. In all application examples (except problem A3), the gas was assumed to be 100% CH_4.

5.1. Problem A1: Gas Production From a Shale Gas Reservoir Using a Horizontal Well

This T+G study focuses on a Cartesian 3D stencil of a horizontal well section that is typical of a Type I shale gas system (Figure 7), as defined and investigated by Freeman (2010) and Moridis et al. (2010). Such systems involve the (usually hydraulically)

induced primary fractures (PF), the undisturbed matrix, and the stress release fractures around the well. The data used in this simulation were as in Freeman (2010). The surface area of the Cartesian system at the well was corrected to reflect its cylindrical geometry. The simulated 3D domain (Figure 7) represents the stencil of the horizontal well system, i.e., the smallest repeatable subdomain that can accurately describe the system behavior. Studies by Olorode (2011) and (2012) have confirmed that such stencils are accurate representatives of the behavior of the entire system for very long production periods.

The discretization of the 3D domain involved subdivisions as small as mm-scale near the fracture face, and resulted in about 800,000 gridblocks. To develop the mesh file, we used an expanded version of the MESHMAKER facility available to the TOUGH+ code (Moridis et al., 2008) and its MINC option (Pruess, 1983), in addition to a short FORTRAN code written for this purpose. Two different media were considered: the matrix and the hydraulically-induced fracture, which was represented by appropriate flow and thermal properties. The problem was solved both isothermally and non-isothermally. The gas was 100% CH_4, and its sorption onto the shale followed an equilibrium Langmuir isotherm (see Equation 4).

Using the T+G code and assuming isothermal conditions, the predicted production rate when the well is operated at a constant bottomhole pressure P_w is shown in Figure 8, which also lists the data used in the simulation. Here, and in Problem A2, we employ the the dimensionless variables commonly used in such studies, which are defined as:

$$t_D = \frac{k}{\varphi \mu c_t x_f^2} \frac{1}{[1+V_L]}\, t,\ q_D = \frac{B\mu}{kh(p_i - p_{wf})}\, q, \quad \text{..... (40)}$$

$$q_{Di}(t) = \frac{1}{t}\int_0^t q_D(\tau)\, d\tau, \ \text{ and } \ q_{Did}(t) = -t\frac{dq_{Di}}{dt} \text{ ..... (41)}$$

Figure 9 shows the distribution of the normalized pressure in the vicinity of the fracture face on the (x,y) plane along the length of the fracture at a height of 4 m above the well plane. Note the steep pressure gradients perpendicular to the fracture face that are the result of the very low permeability of the shale.

The T+G results were identical to those from the T+GW simulations. The differences between the predictions from the isothermal and the non-isothermal simulations were very small, became perceptible at late times, and cannot register as different on the log-log plots (such as the one in Figure 8) typically used in such studies.

5.2. Problem A2: Gas Production From a Shale Gas Reservoir With a Complex Fracture System Using a Horizontal Well

Problem A2 is a sensitivity analysis study that aims to determine the effects of more complex fracture regimes. These are represented by Types II, III and IV (Figure 10), which include secondary planar fractures (generally perpendicular to the primary fractures), natural fractures, and all types of fractures, respectively. Type IV is the most complex system to describe, simulate and analyze. The data in these simulations were as in Freeman (2010). These complex systems involved three individual subdomains, each with appropriate properties: the matrix, the main (hydraulically-induced) fracture, and the secondary planar fractures. The natural fractures were described by a dual-porosity model using the MINC concept (Pruess, 1983) to describe a dual-permeability (as opposed to a dual porosity) model of fracture-matrix interactions.

With the exception of the properties of the various fracture systems, all properties and conditions of the reservoir and of the fluid remained as in Problem A1. The

discretization of the 3D domains included subdivisions as small as mm-scale near the fracture face, and resulted in about a number of gridblocks that varied from about 850,000 elements in the Type II system to about 1,200,000 in the Type IV system. The T+G and T+GW simulations were conducted in both isothermal and non-isothermal mode.

The T+G and T+GW results coincided, and are shown in Figure 11 (which includes the Type I predictions for reference). The four domain types exhibit very different production patterns and performance. The significant discrepancies of the various production estimates indicates the importance of the additional fractures on production and clearly demonstrate that a good grasp of the fracture regime is needed for accurate estimates of production. The obvious conclusion is that simplification of the description of the fracture system by resorting to the simplest type can yield results that significantly underestimate early (and usually the most important) production. Type IV exhibits the highest early production because of its maximum surface area and the largest number of flow pathways to the well, but it also exhibits among the fastest production declines because of exhaustion of the gas and its slow replenishment from sorption. Types II and III exhibit intermediate behavior. As in problem A1, consideration of thermal effects in the simulations yielded insignificant differences in the production estimates.

5.3. Problem A3: Flowing Gas Composition Changes in Shale Gas Wells

Here we investigate compositional changes over time in gas produced from a shale reservoir. The mole fractions of the individual gas components in the initial mixture composition was: Y = 80% CH_4, 7% C_2H_6, 5% C_3H_8, 5% C_4H_{10}, 2% C_5H_{12} and 1%

C_6H_{16}. This composition information, as well as the Langmuir sorption parameters, are listed in Table 8, and the sorption behavior of the various gas components is shown in Figure 12. A Type I system was assumed, and the domain had the configuration, dimensions and discretization of Problem A1. The system characteristics, properties and conditions are as described in Freeman et al. (2012), and are shown in Table 9. Gas was produced at a constant bottomhole pressure p_{wf}.

The identical T+G and T+GW results in Figure 13 include both (a) the flow rate, which shows the slope of -½ typical of fractured shale reservoirs, and (b) the compositional deviation of the produced gas over time. It is noteworthy that the evolution of the gas composition over time clearly shows inflection points that correlate perfectly with the times at which significant changes occur in the gas flow regime in the shale.

5.4. Problem A4: Gas rising through a long fracture from a shale gas reservoir to a shallow aquifer

In this case, the system is composed of three domains: (1) a permeable 100 m thick aquifer and (2) a 100 m thick gas-bearing shale layer, separated by (3) an 200 m-thick impermeable overburden. A vertical water well is located in the aquifer producing at a constant pressure p_{wf}, and a horizontal shale gas well is located in the shale layer. A single long fracture penetrates the entire vertical interval, connecting the shale and aquifer layers. The pressure distribution in the entire system is hydrostatic, and the temperature distribution follows the geothermal gradient of $dT/dz = 0.03\ ^{o}C/m$.

The very complex unstructured grid of this 3D domain was developed using a new Voronoi grid facility, includes about 67,000 elements and is shown in Figure 14. The T+GW code is used for this simulation, which had to be conducted non-isothermally because of the significant temperature range across the system profile. Other properties and conditions of the system are listed in Table 10. The initialization process before the onset of water withdrawal from the water well returns the correct pressure and temperature distribution. Figures 15 shows the initial pressure distribution in the reservoir, which becomes much better defined in the fracture because of the very fine discretization in this subdomain. With the onset of water production, the change in the pressure regime in the aquifer begins to affect flow through the fracture. This results in complex pressure and flow regimes, with initial counterflow of the two phases near the shale layer because of water drainage and gas buoyancy. Figure 16 shows the gas saturation distribution within the fracture after 255 days of water production.

6. Summary and Discussion

We discuss the T+G and T+GW additions to the TOUGH+ family of public domain codes. T+GW describes the non-isothermal two-phase flow of water and a real gas mixture of up to 9 components in a gas reservoir (including a tight/shale gas one), and accounts for coupled flow and thermal effects in porous and/or fractured media, gas behavior, inertial (Klinkenberg) effects, full micro-flow treatment, Darcy and non-Darcy flow through the matrix and fractures of fractured media, gas sorption onto the grains of the porous media, etc. T+G has the same general capabilities, but does not include water, thus describing a single-phase, dry-gas system.

We validate the codes against available analytical and semi-analytical solutions. We show the code capabilities in a series of problems of increasing complexity, ranging from isothermal flow in simpler 1D and 2D conventional gas reservoirs, to non-isothermal gas flow in 3D fractured shale gas reservoirs involving multiple types of fractures, micro-flow, non-Darcy flow and gas composition changes during production.

Because of the T+GW and T+W codes account for practically all known processes and phenomena occurring in ultra-tight systems and involve a minimum of assumptions, they are designed primarily for scientific investigations at any temporal and spatial scale. Thus, they can capture the sub-mm scale processes in the immediate vicinity of fracture surfaces from the very first moments of the onset of production to the end of production, in addition to being able to easily describe the system behavior at a regional scale. Of particular importance is the code capability to describe the distinct compositional behavior, and the shifts in the reservoir and produced gas composition over time, as dictated by the different thermophysical, sorption and transport properties of the individual gases. We believe that the T+GW and T+G codes are powerful tools for the analysis of compositional behavior in gas-rich reservoirs and particularly ultra-tight ones, for testing hypotheses and gaining insights in the evaluation of dominant flow and transport mechanisms, for parameter estimation through history-matching (optimization) processes, for reserve estimation and for production forecasting.

In addition to its benefits to the analysis of hydrocarbon gas reservoirs, it is important to indicate that the T+GW code is fully applicable to a wide variety of other problems, including environmental studies on the impact of escaping gaseous hydrocarbons into overlying potable water aquifers (see problem A4), the study of the geological storage of

greenhouse gas mixtures, and the investigation of the performance of geothermal reservoirs with multi-component non-condensable gas mixtures. Although most of issues were not included in this study, they are to be included in future publications on the range of applications of T+GW.

There are several ideas about inclusion of additional options and capabilities into the T+GW. Expansion of the library of non-condensable gases (and the corresponding number of equations) is a relatively simple endeavor. Accounting for brines (by adding a mass balance equation for salts) is currently the highest priority. The addition of capabilities to handle condensable hydrocarbon gases is also a high-priority, as this would allow the study of production of retrograde gases (condensates) that are of high economic importance.

Acknowledgements

The research described in this article has been funded by the U.S. Environmental Protection Agency through Interagency Agreement (DW-89-92235901-C) to the Lawrence Berkeley National Laboratory, and by the Research Partnership to Secure Energy for America (RPSEA - Contract No. 08122-45) through the Ultra-Deepwater and Unconventional Natural Gas and Other Petroleum Resources Research and Development Program as authorized by the US Energy Policy Act (EPAct) of 2005. The views expressed in this article are those of the author(s) and do not necessarily reflect the views or policies of the EPA.

Nomenclature

A	-	surface area, m^2
b	-	Klinkenberg parameter, Pa
B	-	formation volume factor, surface volume/reservoir volume
b_f	-	fracture width, m
c	-	exponent of the Freundlich sorption isotherm, dimensionless (see Eq. 6)
c_t	-	total compressibility, Pa^{-1}
C_R	-	heat capacity of the dry rock, J kg^{-1} K^{-1}
c_w	-	water compressibility, Pa^{-1}
D^i_K	-	Knudsen diffusivity of species g^i, m^2/s
D^κ_β	-	multicomponent molecular diffusion coefficient of component κ in phase β in the absence of a porous medium, m^2 s^{-1}
D_e^{ij}	-	effective gas (binary) diffusivity of species g^i in species g^j, m^2 s^{-1}
E_i	-	the Exponential Integral function
F_{CD}	-	fracture conductivity, dimensionless
$\mathbf{F}_\beta$	-	the flow vector of phase β, kg $m^{-2}s^{-1}$
$\mathbf{F}^\kappa$, $\mathbf{F}^\kappa{}_\beta$	-	the flow vector of component κ, and of component κ in phase β, kg $m^{-2}s^{-1}$
$\mathbf{g}$	-	gravitational acceleration vector, ms^{-2}
f□	-	fracture void fraction, dimensionless
f_σ	-	radiance emittance factor, dimensionless
h	-	reservoir thickness, m
h^κ_β	-	specific enthalpy of component κ in phase β, J kg^{-1}
H^i	-	Henry's constant (factor) of species g^i in H_2O, Pa
H_{dep}	-	specific enthalpy departure of the gas mixture, J kg^{-1}
U^i_{sol}	-	specific enthalpy of dissolution of gas component g^i in H_2O, J kg^{-1}
H_β	-	specific enthalpy of phase β, J kg^{-1}
$\boldsymbol{J}^\kappa_\beta$	-	diffusive mass flux of component k in phase β, kg m^{-2} s^{-1}
k	-	permeability, m^2 (□m^2 for Cinco-Meng solution)
k_g	-	Klinkenberg-adjusted permeability, m^2
k_∞	-	absolute matrix permeability, m^2
k_f	-	fracture permeability, m^2
k^i_F	-	kinetic coefficients of the Freundlich sorption isotherm, s^{-1} (see Eq. 6)
K^i_F	-	distribution coefficient of the Freundlich sorption isotherm of gas g^i, Pa^{-c}
k_L	-	kinetic constant of the Langmuir sorption, s^{-1}
k^i_l	-	kinetic coefficient of the linear sorption isotherm, s^{-1} (see Eq. 5)
K^i_l	-	distribution coefficient of the linear sorption isotherm of gas g^i, Pa^{-1}
$\bar{k}_\theta$	-	composite thermal conductivity of the fluids-impregnated rock, W m^{-1} K^{-1}
l	-	fracture spacing, m
m_L	-	Langmuir isotherm parameter, kg of gas/kg of matrix (see Eq. 3)
n	-	number of normal sets of fractures, dimensionless
$\mathbf{n}$	-	the inward unit normal vector
N_G	-	number of gaseous components in the water-free gas mixture
N^i_D	-	molar flux of component g^i, $mole/m^2/s$
p	-	pressure, Pa
p_b	-	base pressure reference point for pseudo-pressure computation, Pa
P_{cGA}	-	gas-water capillary pressure, Pa

p_D - dimensionless pressure
p_{dc} - conversion factor (= 2π in SI units)
p_{dg} - dry gas pressure, Pa
p_k - Klinkenberg-adjusted pressure, Pa
p_L - Langmuir isotherm parameter, Pa (see Eq. 3)
p_r - pressure at radius r, Pa
p^v - partial pressure of water vapor, Pa
q - mass flow rate, kg s^{-1}
q^θ - rate of heat addition/withdrawal, W kg^{-1}
r - radius, m
r_D - dimensionless radius
r_e - outer boundary radius, m
r_w - wellbore radius, m
t - time, s
T - temperature, K
t_D - dimensionless time
u^i - ideal part of specific internal energy of sorbed gas component g^i, J kg^{-1}
$(u^i)_*$ - total specific internal energy of sorbed gas component g^i, including departure effects, J kg^{-1}
U_{dep} - specific internal energy departure of the gas mixture, J kg^{-1}
U^i_{sol} - specific internal energy of dissolution of gas component g^i in H_2O, J kg^{-1}
U_β - specific internal energy of phase β, J kg^{-1}
$\mathbf{v}_\beta$ - flow velocity of phase β, ms^{-1}
V, V_n - the volume and volume of subdomain n, respectively, m^3
V_p - pore volume, m^3
x_f - fracture half-length, m
Z - gas compressibility factor, dimensionless

Greek Symbols

α - block shape factor, $1/m^2$
α_K - Knudsen-related parameter (see Eq. 29)
β - denotes phases, β = A, G
β_β - parameter for Forchheimer flow of phase β □□□□□□1□
γ - permeability reduction factor, dimensionless
Γ_n - the surface of subdomain n [m^2],
δ - fracture aperture, m
κ - denotes the component κ
λ - Warren and Root interporosity flow parameter, dimensionless
$\bar{\lambda}$ - mean free path of gas molecules, m
μ - viscosity, Pa-s
τ_G - gas tortuosity, dimensionless
ϕ - porosity, dimensionless
Φ_β - total pressure, Pa (see Eq. 11)
ψ - pseudo-pressure (see Eq. 28)
Ψ^i - mass of sorbed component g^i per unit mass of rock, kg/kg

ω	-	Warren and Root storativity ratio, dimensionless

Subscripts

0		denotes initial conditions
A	-	aqueous
abs	-	implies that the property reflects an absolute media value
cont	-	implies that the property reflects an equivalent continuum-adjusted value
f	-	fracture
G	-	gas
m	-	matrix
pore	-	indicates pore-associated property
r	-	denotes a reference state
w	-	denotes a well (source or sink)

References

Americal Petroleum Institute (API). Policy Issues: Facts about Shale Gas 2013. http://www.api.org/policy-and-issues/policy-items/exploration/facts_about_shale_gas

Anderson, D.M., Nobakht, M., Moghadam, S. et al. 2010. Analysis of Production Data from Fractured Shale Gas Wells. Paper SPE 131787 presented at the SPE Unconventional Gas Conference, Pittsburgh, Pennsylvania, USA. doi: 10.2118/131787-MS

Barree R.D., and M.W. Conway, Multiphase non-Darcy flow in proppant packs, Paper SPE 109561, 2007 Annual Technical Conference and Exhibition, Anaheim, CA, 11–14 Nov 2007.

Bello, R.O. and Wattenbarger, R.A. 2008. Rate Transient Analysis in Naturally Fractured Shale Gas Reservoirs. Paper SPE 114591 presented at the CIPC/SPE Gas Technology Symposium 2008 Joint Conference, Calgary, Alberta, Canada. doi: 10.2118/114591- MS

Bird, R.B., W.E. Stewart, and E.N. Lightfoot, *Transport Phenomena*. New York: John Wiley & Sons, Inc., 2007.

Blasingame, 1993. T.A., Semi-Analytical Solutions for a Bounded Circular Reservoir – No Flow and Constant Pressure Outer Boundary Conditions: Unfractured Well Case, Paper SPE 25479, SPE Production Operations Symposium, Oklahoma City, Oklahoma, 21-23 March 1993.

Blasingame, T.A. and Poe Jr., B.D. 1993. Semianalytic Solutions for a Well with a Single Finite-Conductivity Vertical Fracture. Paper SPE 26424 presented at the SPE Annual Technical Conference and Exhibition, Houston, Texas, USA. doi: 10.2118/26424-MS.

Chung, T.H., M. Ajlan, L.L. Lee, K.E. Starling. Generalized multiparameter correlation for nonpolar and polar fluid transport properties, *Ind. Eng. Chem. Res*., **27**(4), 671-679, 1988 (doi: 10.1021/ie00076a024)

Cinco-Ley, H. and Meng, H.-Z. 1988. Pressure Transient Analysis of Wells With Finite Conductivity Vertical Fractures in Double Porosity Reservoirs. Paper SPE 18172-MS presented at the SPE Annual Technical Conference and Exhibition, Houston, Texas, 2-5 October 1988. http://dx.doi.org/10.2118/18172-MS.

Cinco-Ley, H., F. Samaniego, and N. Dominguez, 1978. Transient pressure behavior for a well with a finite-conductivity vertical fracture, *SPE Journal* **18**(4): 253-264. SPE 6014-PA. http://dx.doi.org/10.2118/6014-PA

Cipolla, C.L., Lolon, E., Erdle, J. et al. 2009. Modeling Well Performance in Shale-Gas Reservoirs. Paper SPE 125532 presented at the SPE/EAGE Reservoir Chara- cterization and Simulation Conference, Abu Dhabi, UAE. doi: 10.2118/125532-MS

Civan, F., Effective Correlation of Apparent Gas Permeability in Tight Porous Media. *Transp. in Porous Med.*, 2008 (doi: 10.1007/s11242-009-9432-z)

Clarkson, C.R. and R.M. Bustin, Binary gas adsorption/desorption isotherms: effect of moister and coal composition upon carbon dioxide selectivity over methane. *International Journal of Coal Geology*, **42**, 241-271, 1999.

Computer Modeling Group (CMG). 2013 GEM General Release (GEM 2013.10), http://www.cmgl.ca/software/soft-gem

Dietz, D.N.. Determination of Average Reservoir Pressure From Build-Up Surveys. *JPT*, 955-959, 1965.

Doronin, G.G. and N.A. Larkin. On dusty gas model governed by the Kuramoto-Sivashinsky equation. *Computational and Applied Mathematics*, **23**(1), 67-80, 2004.

Edwards, A.L.. TRUMP: A Computer Program for Transient and Steady State Temperature Distributions in Multidimensional Systems, National Technical Information Service, National Bureau of Standards, Springfield, VA, 1972.

Finsterle, S.. Implementation of the Forchheimer Equation in iTOUGH2, Project Report, Lawrence Berkeley National Laboratory, Berkeley, Calif., 2001.

Forchheimer, P., Wasserbewewegung durch Boden, *ZVDI* 45, 1781, 1901.

Fraim, M.L., and R.A. Wattenbarger. Gas Reservoir Decline Curve Analysis Using Type Curves with Real Gas Pseudopressure and Pseudotime, *SPEFE*, 671-682, 1987.

Freeman, C.M.. Study of flow regimes in multiply-fractured horizontal wells in tight gas and shale gas reservoir systems, M.Sc. Thesis, Petroleum Engineering Department, Texas A&M University, 2010.

Freeman, C.M., Moridis, G.J., Ilk, D. et al. 2009. A Numerical Study of Performance for Tight Gas and Shale Gas Reservoir Systems. Paper SPE 124961 presented at the SPE Annual Technical Conference and Exhibition, New Orleans, Louisiana, USA. doi: 10.2118/124961-MS.

Freeman, C.M., G.J. Moridis, and T.A. Blasingame. A Numerical Study of Microscale Flow Behavior in Tight Gas and Shale Gas Reservoir Systems. *Transp. in Porous Med., 90*(1): 253-268, 2011 (doi: 10.1007/ s11242-011-9761-6)

Freeman, C.M., G.J. Moridis, E. Michael, and T.A. Blasingame. Measurement, Modeling, and Diagnostics of Flowing Gas Composition Changes in Shale Gas Wells, Paper SPE 153391, SPE Latin American and Caribbean Petroleum Engineering Conference, Mexico City, Mexico, 16-18 April, 2012.

Freeman, C.M., G.J. Moridis, D. Ilk, and T.A. Blasingame, A Numerical Study of Performance for Tight Gas and Shale Gas Reservoir Systems, *Journal of Petroleum Science and Engineering*, **108**, 22-39, 2013 (http://dx.doi.org/10.1016/j.petrol. 2013.05.007).

Fuller, E.N., P.D. Schettler, and J.C. Giddings. A new method for prediction of binary gas-phase diffusion coefficients, Ind. Eng. Chem., **58**, 19–27, 1966.

Gao, C., J.W. Lee, J.P. Spivey, and M.E. Semmelbeck. Modeling multilayer gas reservoirs including sorption effects, SPE paper 29173, SPE Eastern Regional Conference & Exhibition, Charleston, West Virginia, 8-10 November, 1994.

Gringarten, A.C. 1971. Unsteady-State Pressure Distributions Created by a Well with a Single Horizontal Fracture, Partial Penetration, or Restricted Entry. Ph.D. Dissertation, Stanford University, Stanford, California, USA.
Gringarten, A.C., Henry J. Ramey, J., and Raghavan, R. 1974. Unsteady-State Pressure

Distributions Created by a Well with a Single Infinite-Conductivity Vertical Fracture. *SPE Journal* **14** (4). doi: 10.2118/4051-PA.

Houze, O., Tauzin, E., Artus, V. et al. 2010. The Analysis of Dynamic Data in Shale Gas Reservoirs - Part 1. Company report, Kappa Engineering, Houston, Texas, USA.
International Formulation Committee (IFC). A Formulation of the Thermodynamic Properties of Ordinary Water Substance, IFC Secretariat, Düsseldorf, Germany, 1967.

Jayakumar, R., Sahai, V., and Boulis, A. 2011. A Better Understanding of Finite Element Simulation for Shale Gas Reservoirs through a Series of Different Case Histories. Paper SPE 142464 presented at the SPE Middle East Unconventional Gas Conference and Exhibition, Muscat, Oman. doi: 10.2118/142464-MS

Jones, S. C., A rapid accurate unsteady-state Klinkenberg parameter, *SPE Journal* 383–397, 1972.

Katz, D. L. et al., *Handbook of Natural Gas Engineering*. McGraw-Hill, New York, 1959.

Kim, J., and G.J. Moridis. Development of the T+M coupled flow-geomechanical simulator to describe fracture propagation and coupled flow-thermal-geomechanical processes in tight/shale gas systems, *Computers & Geosciences, 60*, 184-198, 2013 (doi: 10.1016/j.cageo.2013.04.023)**.**

Klinkenberg, L.J. The Permeability of Porous Media to Liquid and Gases, Proceedings, *API Drilling and Production Practice*, 200-213, 1941.

Mattar, L. 2008. Production Analysis and Forecasting of Shale Gas Reservoirs: Case History-Based Approach. Paper SPE 119897 presented at the SPE Shale Gas Production Conference, Fort Worth, Texas, USA. doi: 10.2118/119897-MS

Medeiros, F., Ozkan, E., and Kazemi, H. 2006. A Semianalytical, Pressure-Transient

Model for Horizontal and Multilateral Wells in Composite, Layered, and Compartmentalized Reservoirs. Paper SPE 102834 presented at the SPE Annual Technical Conference and Exhibition, San Antonio, Texas, USA. doi: 10.2118/102834-MS.

Miller, M.A., Jenkins, C.D., and Rai, R.R. 2010. Applying Innovative Production Modeling Techniques to Quantify Fracture Characteristics, Reservoir Properties, and Well Performance in Shale Gas Reservoirs. Paper SPE 139097 presented at the SPE Eastern Regional Meeting, Morgantown, West Virginia, USA. doi: 10.2118/139097- MS.

Millington, R.J., and J.P. Quirk. Permeability of porous solids, *Trans. Faraday Soc*., **57**, 1200-1207, 1961.

Moridis, G.J., M. Kowalsky and K. Pruess. TOUGH+HYDRATE v1.0 User's Manual. LBNL-161E, Lawrence Berkeley National Laborotory, Berkeley, Calif., 2008. Moridis, G.J., T.A. Blasingame, and C.M. Freeman. Analysis of Mechanisms of Flow in Fractured Tight-Gas and Shale-Gas Reservoirs, Paper SPE 139250, SPE Latin American & Caribbean Petroleum Engineering Conference, Lima, Peru, 1–3 December 2010.

Mouawad, J. Estimate places natural gas reserves 35% higher, *New York Times*, 17 June 2009

Narasimhan, T.N., P.A. Witherspoon and A.L. Edwards. Numerical Model for Saturated-Unsaturated Flow in Deformable Porous Media, Part 2: The Algorithm, *Water Resour. Res.*, **14**(2), 255-261, 1978.

Odunowo, T.O.. Numerical Simulation Study To Investigate Expected Productivity Improvement Using The "Slot-Drill" Completion, M.Sc. Thesis, PetroleumEngineering Department, Texas A&M University, 2012.

Olorode, O., Numerical Modeling and Analysis of Shale-Gas Reservoir Performance Using Unstructured Grids, M.Sc. Thesis, Petroleum Engineering Department, Texas A&M University, 2011.

Peng, D.Y., and D.B. Robinson. A New Two-Constant Equation of State, *Indust. and Engr. Chemistry: Fundamentals* **15**, 59-64, 1976.

Pruess, K.. GMINC - A Mesh Generator for Flow Simulations in Fractured Reservoirs, Lawrence Berkeley Laboratory Report LBL-15227, Berkeley, CA, 1983.

Pruess, K.. ECO2M: A TOUGH2 Fluid Property Module for Mixtures of Water, NaCl, and CO_2, Including Super- and Sub-Critical Conditions, and Phase Change Between Liquid and Gaseous CO_2, Lawrence Berkeley National Laboratory Report LBNL-4590E, Berkeley, CA, 2011.

Pruess, K. and K. Karasaki. A Practical Method for Modeling Fluid and Heat Flow in Fractured Porous Media. Paper SPE 10509, Sixth SPE Symposium on Reservoir Simulation, New Orleans, LA, Feb. 1-3, 1982.

Pruess, K., and T.N. Narasimhan. On Fluid Reserves and the Production of Superheated Steam from Fractured, Vapor-Dominated Geothermal Reservoirs, *J. Geophys. Res.*, **87**(B11), 9329 – 9339,1982.

Pruess, K. and T.N. Narasimhan. A Practical Method for Modeling Fluid and Heat Flow in Fractured Porous Media, *Soc. Pet. Eng. J.*, **25**(1), 14-26, 1985.

Pruess, K., C. Oldenburg, and G. Moridis. *TOUGH2 User's Guide, Version 2.0*, Report LBNL-43134, Lawrence Berkeley National Laboratory, Berkeley, Calif., 1999.

Redlich, O., and J.N.S. Kwong. On The Thermodynamics of Solutions, *Chem. Rev.* **44** (1): 233–244, 1949.

Riazi, R. and C.H. Whitson. Estimating diffusion coefficients of dense fluids, Ind. Eng. Chem. Res., **32**, 3081-3088, 1993.

Rutqvist J. and C.-F Tsang. A Study of Caprock Hydromechanical Changes Associated with CO_2 Injection into a Brine Aquifer. *Environmental Geology*, **42**, 296-305, 2002.

Schettler, P.D., and C.R. Parmely, Contributions to total storage capacity in devonian shales, SPE paper 23422, SPE Eastern Regional Meeting, Lexington, Kentucky, 22-25 October, 1991.

Sclumberger (SLB) Software, 2013 ECLIPSE for Unconventionals, http://www.software.slb.com/products/foundation/pages/eclipse-unconventionals.aspx

Soave, G.. Equilibrium constants from a modified Redlich–Kwong equation of state, *Chemical Engineering Science* **27** (6): 1197–1203, 1972.

U.S. DOE, Modern Shale Gas Development in the United States: A Primer, 2009. http://www.netl.doe.gov/technologies/oilgas/publications/EPreports/Shale_Gas_Primer_2009.pdf

Warlick, D.N.. Gas Shale and CBM Development in North America. Oil and Gas Journal. 3 (11), 2006. 1-8. http://www.ogfj.com/index/article-tools-template/printArticle/articles/oil-gas-financial-journal/volume-3/issue-11/features/gas-shale- and-cbm-development-in-north-america.html.

Warren, J.E. and P.J. Root. The Behavior of Naturally Fractured Reservoirs, *SPEJ* 245-55; *Trans*. AIME, **228,** 1963.

Wattenbarger, R.A. and H.J. Ramey. Gas well testing with turbulence, damage and wellbore storage, SPE 1835, *J. Pet. Tech.*, 877-884, 1968.

Webb, S.W. and K. Pruess. The Use of Fick's Law for Modeling Trace Gas Diffusion in Porous Media. *Transport in Porous Media,* **51***,* 327-341, 2003.

Wu, Y., Pruess, K., and P. Persoff. Gas Flow in Porous Media with Klinkenberg Effects. Transport in Porous Media, 32, 117-137, 1988.

Wu, Y.S., B. Lai, J.L. Miskimins, P. Fakcharoenphol and Y. Di. Analysis of Multiphase Non-Darcy Flow in Porous Media, Transport in Porous Media, **88**, 205–223, 2011 (doi: 10.1007/s11242-011-9735-8).

Table 1 — Properties and conditions in Problem V1.

Data Type	Values
Matrix permeability k	3.04×10^{-14} m^2 (30.4 mD)
Reservoir thickness h	10 m
Well radius r_w	0.059 m
Reservoir radius r_e	100 m
Reservoir pressure p	10 MPa
Reservoir temperature T	60 ^{o}C
Reservoir porosity ϕ	0.30
Rock compressibility	2×10^{-10} 1/Pa
Gas composition	100% CH_4
Gas EOS	Peng-Robinson

Table 2 — Properties and conditions in Problem V2.

Data Type	Values
Matrix permeability k	3.04×10^{-14} m^2 (30.4 mD)
Reservoir thickness h	10 m
Well radius r_w	0.059 m
Reservoir radius r_e	100 m
Reservoir pressure p	10 MPa
Reservoir temperature T	30 ^{o}C
Reservoir porosity ϕ	0.30
Total compressibility c_t	4.88×10^{-10} 1/Pa
Gas EOS	Peng-Robinson

Table 3 — Warren and Root dual porosity model properties in Problem V3

p_i	T	q	B	□	h	$k_{f,abs}$	r_w	c_m	c_f
Pa	°C	m^3/s		Pa-s	m	m^2	m	1/Pa	1/Pa
6.08E6	90	2.50E-5	1	3.17E-4	1.00E1	9.26E-11	5.90E-2	1.3E-09	1.00E-7

Table 4 — Porosity and permeability parameters in the Warren and Root and T+G, T+RG computations

	Warren & Root				T+G, T+GW			
Case	□$_m$	□$_f$	k_m	k_f	ϕ_m	ϕ_f	k_m	k_f
			m^2	m^2			m^2	m^2
1	5.00E-02	1.00E-04	1.00E-17	6.17E-15	5.00E-02	1.00E+00	1.00E-17	6.17E-15
2	5.00E-02	1.00E-05	1.00E-17	6.17E-16	5.00E-02	1.00E+00	1.00E-17	6.17E-16

Table 5 —Warren and Root parameters: derived variables of the analytical solution in Problem V3

Case	l_{const}	n	f	δ	α	ω	λ
	m			m	m^{-2}		
1	1	3	0.0001	3.33E-5	60	1.3334E-1	3.38353E-4

Table 6 — Parameters in Problem V4 of Klinkenberg flow

k_∞	b	p_i	μ	ϕ	h	q	c_t	z
m^2	1/Pa	Pa	Pa-s		m	m^3/s	1/Pa	
3.0E-14	73830.6	1.00E7	1.44E-5	0.3	10	1.54E-2	1.07E-7	0.89

Table 7 — Properties and conditions in Problem V5

Case	p_i	k_m	k_f	h	q	B	μ	ϕ_m	c_t	x_f	F_{cD}	b_f
	kPa	□m^2	□m^2	m	m^3/d		Pa.s		1/Pa	m		m
1	1.0E5	3.3E-3	3.0E3	10	172.8	1	4.91E-4	0.3	3.37E-10	20	10^3	0.022
2	1.0E5	3.3E-4	3.0E3	10	172.8	1	4.91E-4	0.3	3.37E-10	20	10^4	0.022

Table 8 — Langmuir and initial composition parameters used in problem A4

Component	Y_i	b_i (1/psi)	V_{Li} (scf/ton)
Methane	0.80	$2.08\text{x}10^{-5}$	$6.9\text{x}10^{1}$
Ethane	0.07	$2.11\text{x}10^{-4}$	$2.59\text{x}10^{2}$
Propane	0.05	$7.02\text{x}10^{-4}$	$5.69\text{x}10^{2}$
Butane	0.05	$3.84\text{x}10^{-3}$	$2.00\text{x}10^{2}$
Pentane	0.02	$8.10\text{x}10^{-3}$	$4.03\text{x}10^{2}$
Hexane	0.01	$1.21\text{x}10^{-2}$	$7.41\text{x}10^{2}$

Table 9 — Reservoir and well system parameters for the North American shale gas play used in Problem A3

Parameters	SI Unit	Field Unit
Fracture half-length, x_f	152.4 m	500 ft
Fracture conductivity,	1310 -	1310 -
Fracture spacing, d_f	15.24 m	50 ft
Reservoir thickness, h	30.48 m	100 ft
Permeability, k_{shale}	$1.0\text{x}10^{-19}$ m^2	$1.0\ \text{x}10^{-4}$ md
Matrix porosity, φ	2.76	2.76
Temperature, T	86.4 ^{0}C	187.52 ^{0}F
Well radius, r_w	0.1 m	0.32 ft
Reservoir pressure, p_i	$3.15\text{x}10^{7}$ Pa	4568
Well pressure, p_{wf}	$2.5\text{x}10^{7}$ Pa	3626

Table 10 — Properties and conditions in Problem A4

Initial Conditions		Shale Permeability	Fracture Permeability	Aquifer Permeability	Water Well Pressure
p	T	k_{shale}	k_{frac}	k_{aqu}	p_{wf}
Geothermal /hydrostatic gradient		m^2	m^2	m^2	Pa
		$3.0\text{x}10^{-19}$	$3.0\text{x}10^{-9}$	$3.0\text{x}10^{-13}$	$5\text{x}10^{6}$

FIGURE CAPTIONS

Figure 1 — Space discretization and geometry data in the integral finite difference method.

Figure 2 — Validation of the T+G and T+GW codes against the analytical solution of Fraim and Wattenbarger (1987) in Problem V1 of real gas transient flow in a cylindrical reservoir.

Figure 3 — Validation of the T+GW code against the analytical solution of Blasingame (1993) in Problem V1 of pseudo-steady-state water flow in a finite cylindrical reservoir.

Figure 4 — Validation of the T+GW code against the analytical solution of Warren and Root (1963) in Problem V3 of flow in a dual-porosity reservoir.

Figure 5 — Validation of the T+G code against the analytical solution of Wu et al. (1988) in Problem V4 of Klinkenberg flow in a cylindrical gas reservoir. The T+G and T+GW solutions are identical.

Figure 6 — Validation of the T+GW code against the analytical solutions of Cinco-Ley and Meng (1988) in Problem V5 of flow into a vertical fracture intersected by a vertical well at its center. Case 1: $F_{CD} = 10^3$; Case 2: $F_{CD} = 10^4$.

Figure 7 — Stencil of a Type I system involving a horizontal well in a tight- or shale-gas reservoir (Moridis et al., 2010).

Figure 8 — Prediction of gas production in Problem A1 (Freeman et al., 2010).

Figure 9 — Pressure distribution in the vicinity of the hydraulically induced fracture in the shale gas system of Problem A1. Note the steep pressure gradient caused by the very low permeability of the shale.

Figure 10 — Stencils of Type II, III and IV systems involving a horizontal well in a tight- or shale-gas reservoir (Moridis et al., 2010).

Figure 11 — Effect of fracture regime on gas production in Problem A2 (Freeman et al., 2010).

Figure 12 — Langmuir sorption isotherms of the various gases in Problem A3.

Figure 13 — Prediction of gas production and compositional changes in Problem A3 (Freeman et al., 2012).

Figure 14 — SeTES output of the spatial distribution of fracture half length (feet).

Figure 14 — The domain discretization of the 3D system in Problem A4. The blue subdomain denotes the vicinity of the vertical water well, the yellow subdomain depicts the vicinity of the horizontal gas production well, and the dark area indicates the fracture.

Figure 15 — Hydrostatic pressure distribution at initialization in the domain of Problem A4.

Figure 16 — Gas saturation distribution in the fracture of Problem A4 at t = 255 days, caused by the rising gas plume.

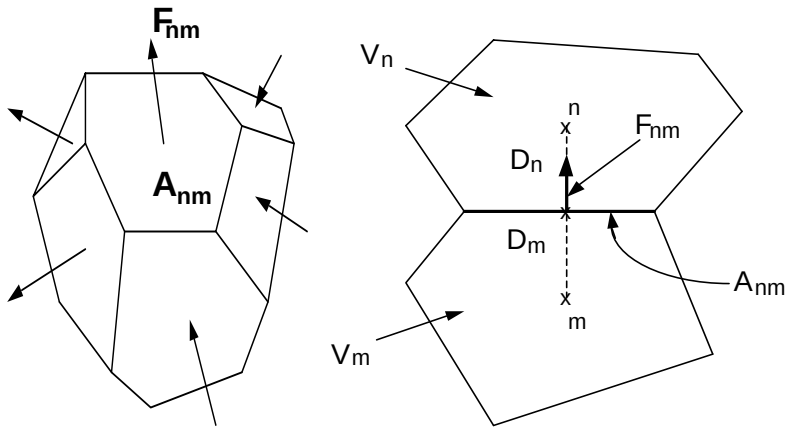

Figure 1 — Space discretization and geometry data in the integral finite difference method.

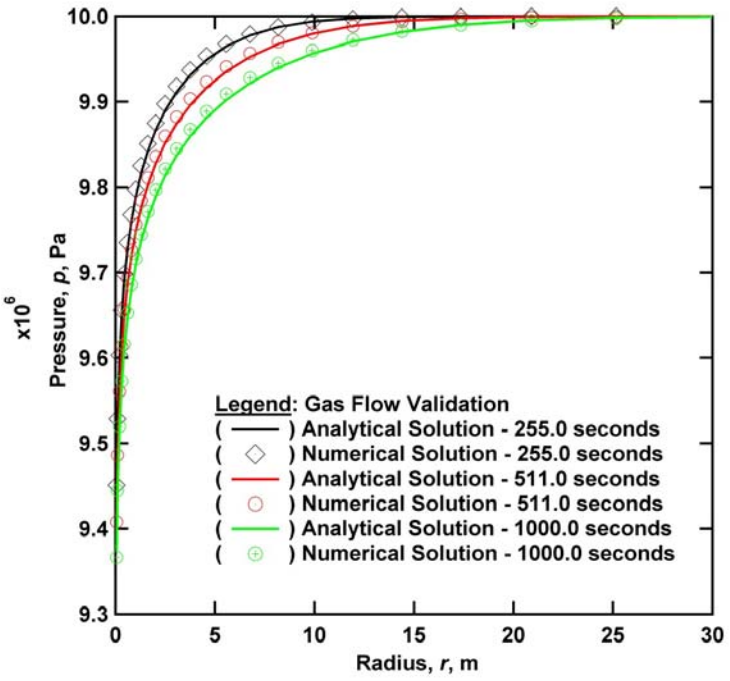

Figure 2 — Validation of the T+G and T+GW codes against the analytical solution of Fraim and Wattenbarger (1987) in Problem V1 of real gas transient flow in a cylindrical reservoir.

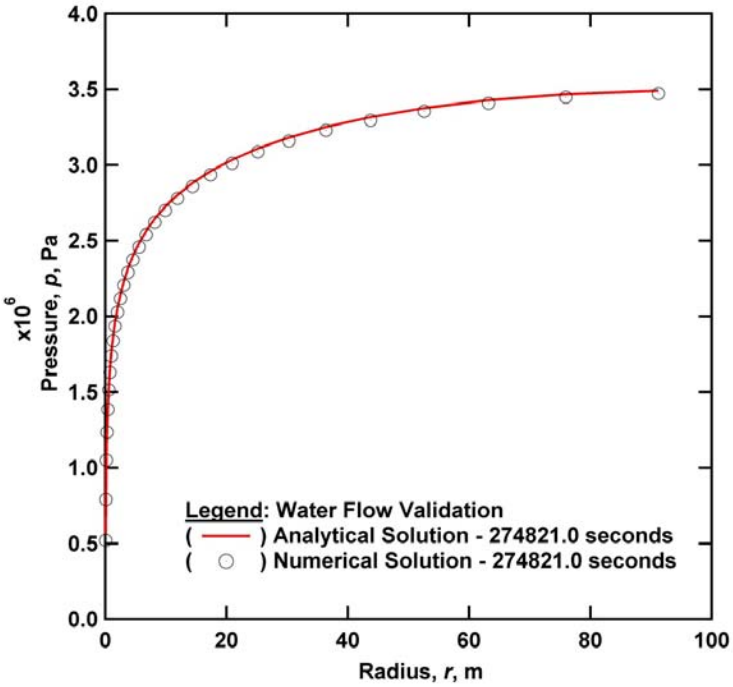

Figure 3 — Validation of the T+GW code against the analytical solution of Blasingame (1993) in Problem V2 of pseudo-steady-state water flow in a finite cylindrical reservoir.

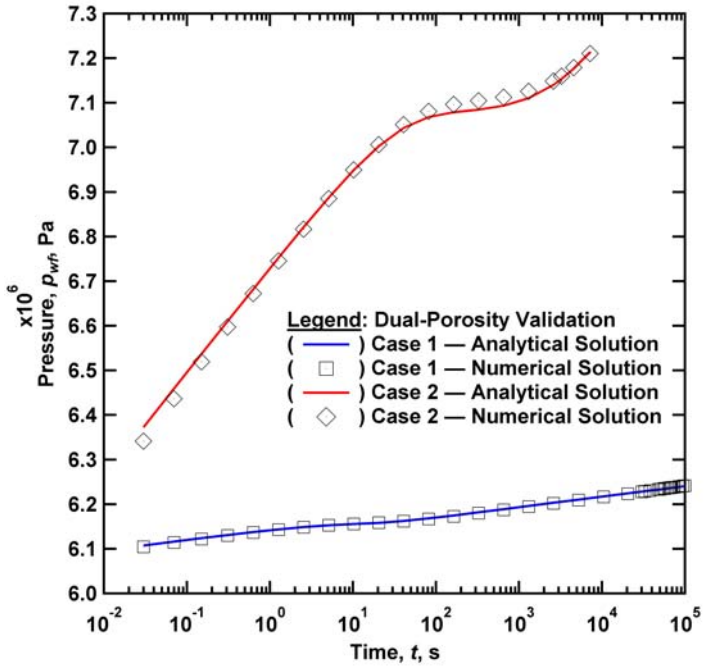

Figure 4 — Validation of the T+GW code against the analytical solution of Warren and Root (1963) in Problem V3 of flow in a dual porosity reservoir (Cases 1 and 2).

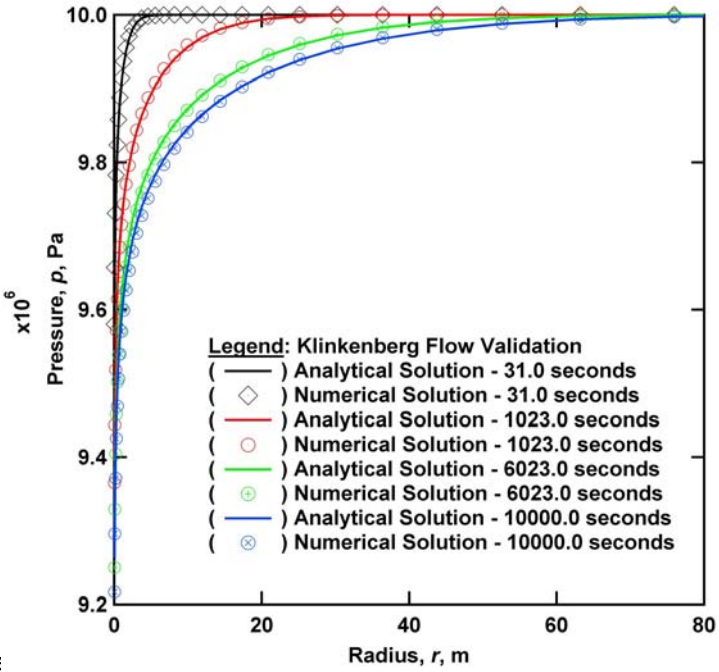

Figure 5 — Valida 1988) in Problem V4 of Klinkenberg flow in a cylindrical gas reservoir. The T+G and T+GW solutions are identical.

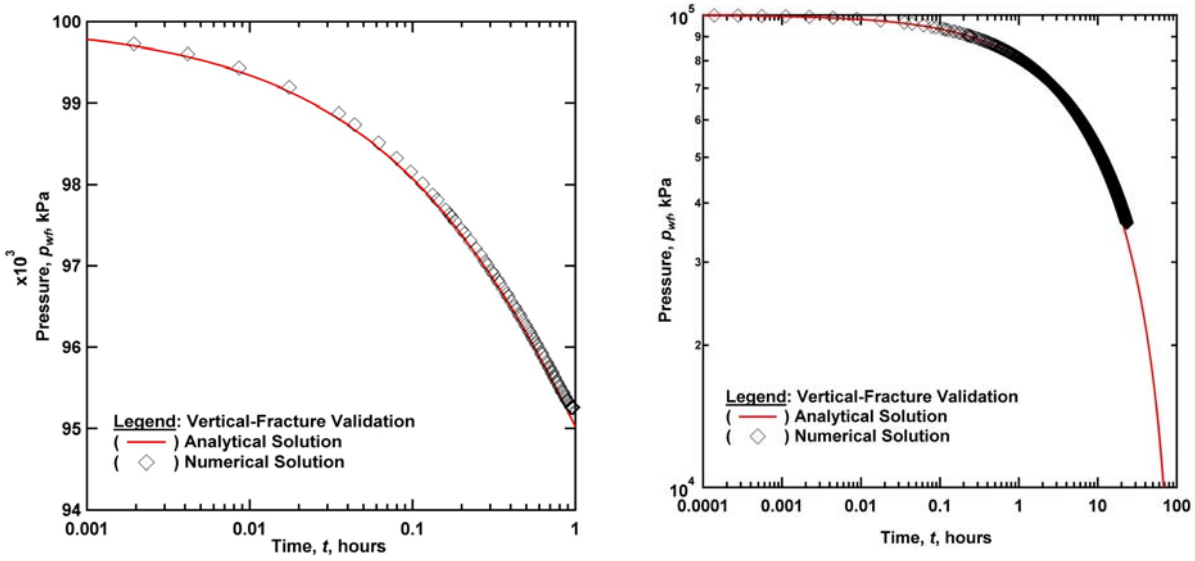

Figure 6 — Validation of the T+GW code against the analytical solutions of Cinco-Ley and Meng (1988) in Problem V5 of flow into a vertical fracture intersected by a vertical well at its center. Case 1: $F_{CD} = 10$; Case 2: $F_{CD} = 10^4$.

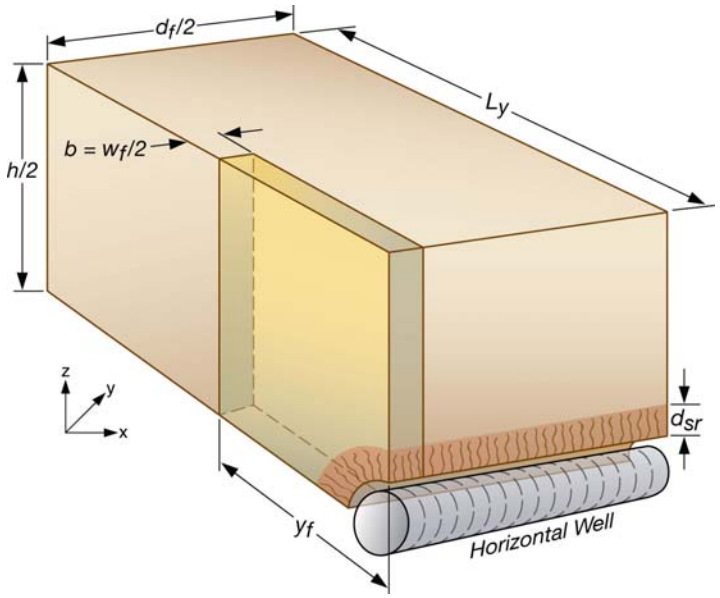

Figure 7 — Stencil of a Type I system involving a horizontal well in a tight- or shale-gas reservoir (Moridis et al., 2010).

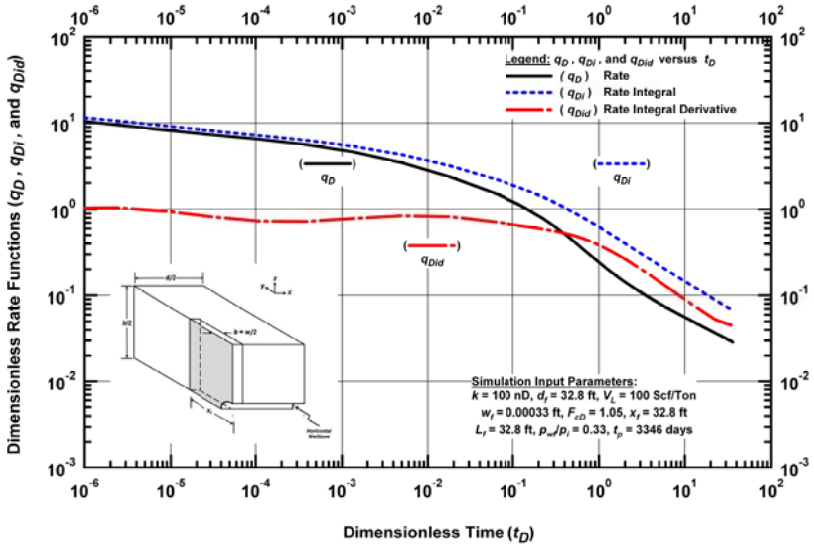

Figure 8 — Prediction of gas production in Problem A1 (Freeman et al., 2010).

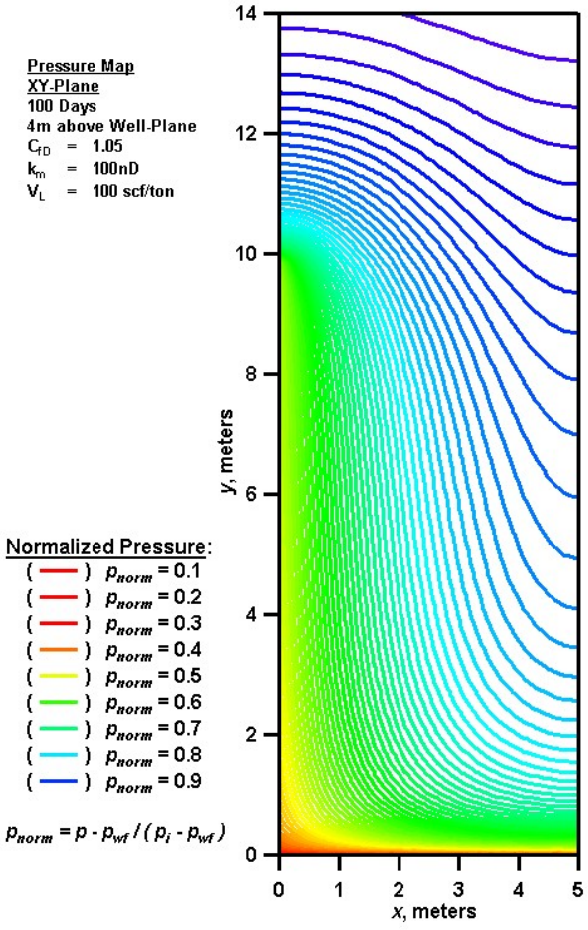

Figure 9 — Pressure distribution in the vicinity of the hydraulically induced fracture in the shale gas system of Problem A1. Note the steep pressure gradient caused by the very low permeability of the shale.

Type II

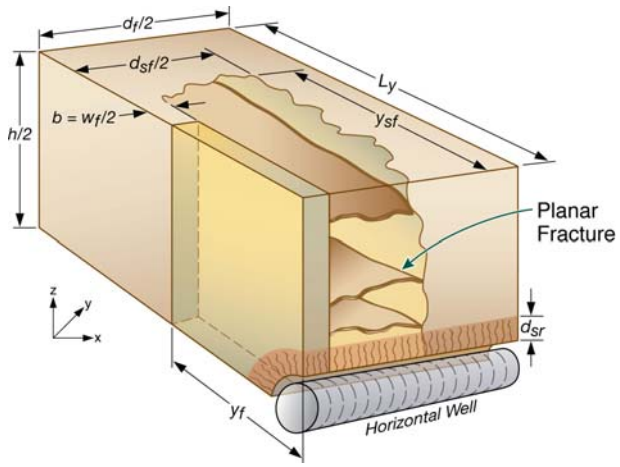

Type III

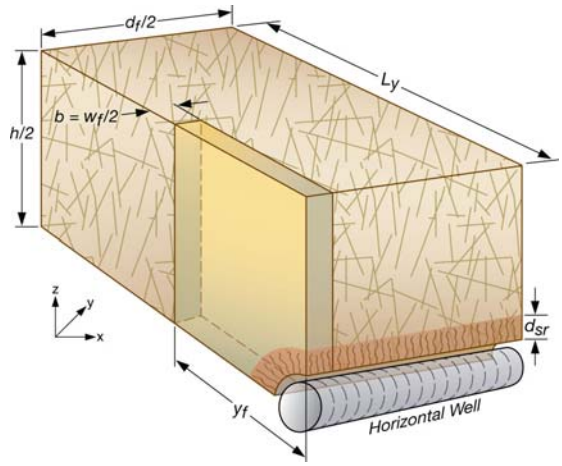

Type IV

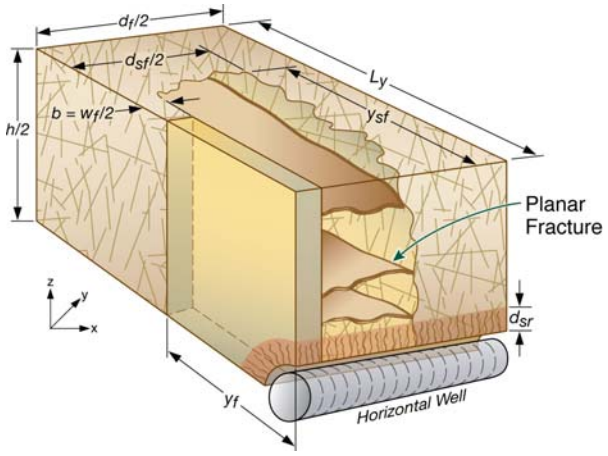

Figure 10 — Stencils of Type II, III and IV systems involving a horizontal well in a tight- or shale-gas reservoir (Moridis et al., 2010).

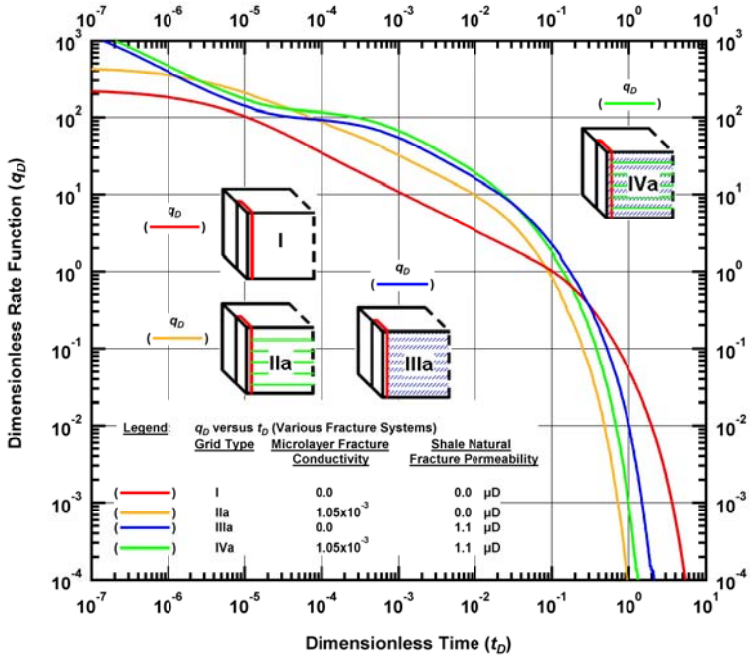

Figure 11 — Effect of fracture regime on gas production in Problem A2 (Freeman et al., 2010).

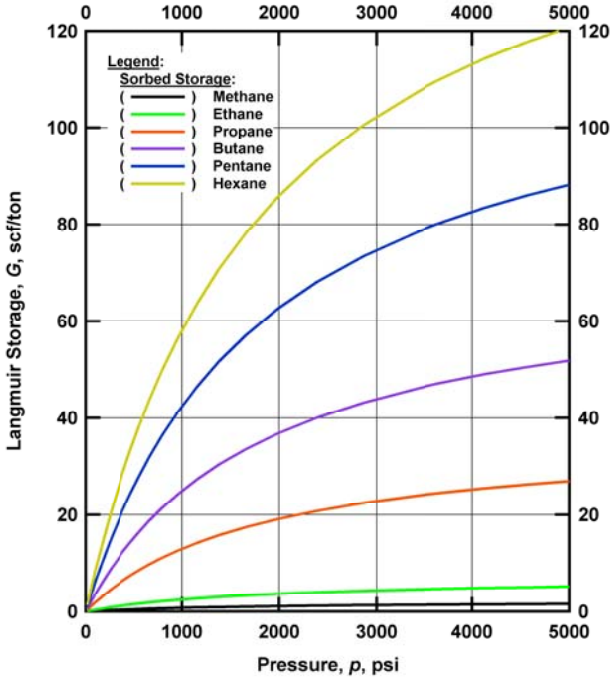

Figure 12 — Langmuir sorption isotherms of the various gases in Problem A3.

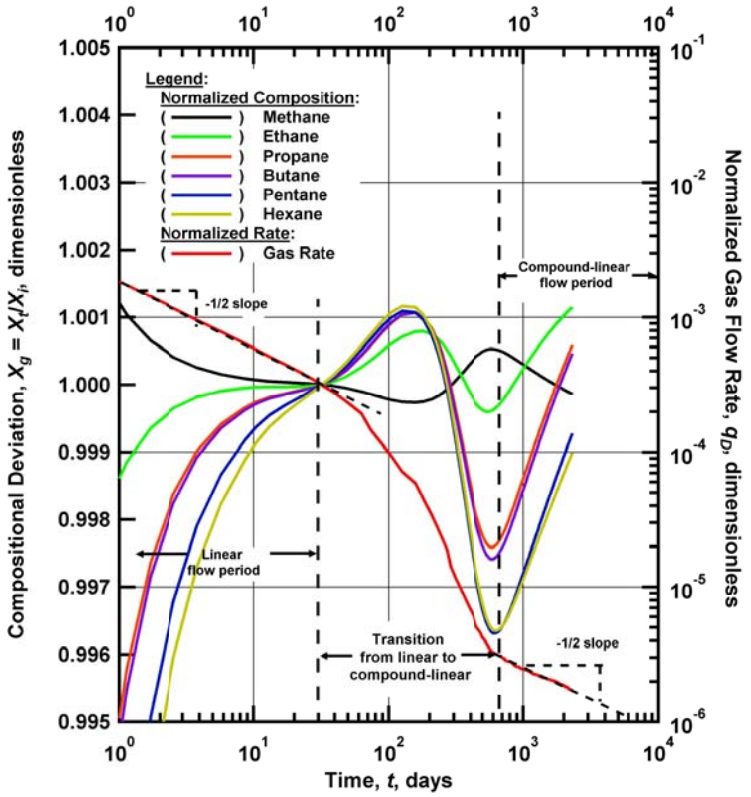

Figure 13 — Prediction of gas production and compositional changes in Problem A3 (Freeman et al., 2012). Note that the onset of the compound-linear flow occurs when the transients of flow into individual fractures begin to interfere with each other.

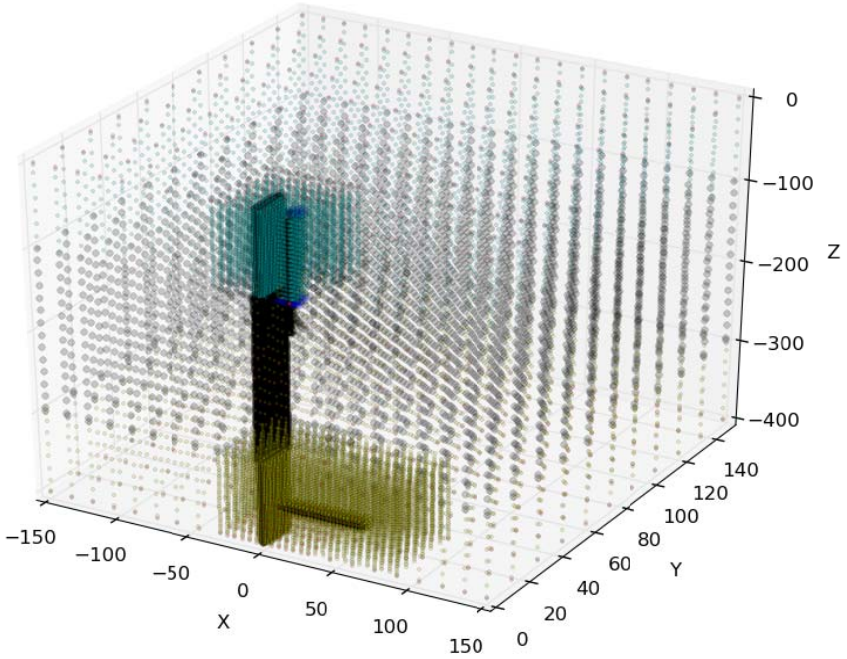

Figure 14 — The domain discretization of the 3D system in Problem A4. The blue subdomain denotes the vicinity of the vertical water well, the yellow subdomain depicts the vicinity of the horizontal gas production well, and the dark area indicates the fracture.

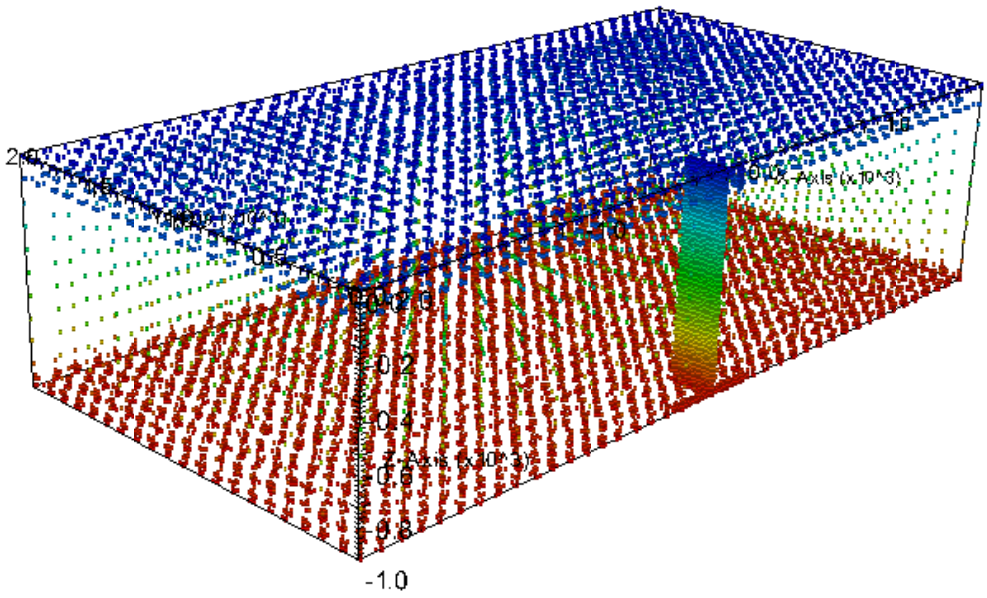

Figure 15 — Hydrostatic pressure distribution at initialization in the domain of Problem A4.

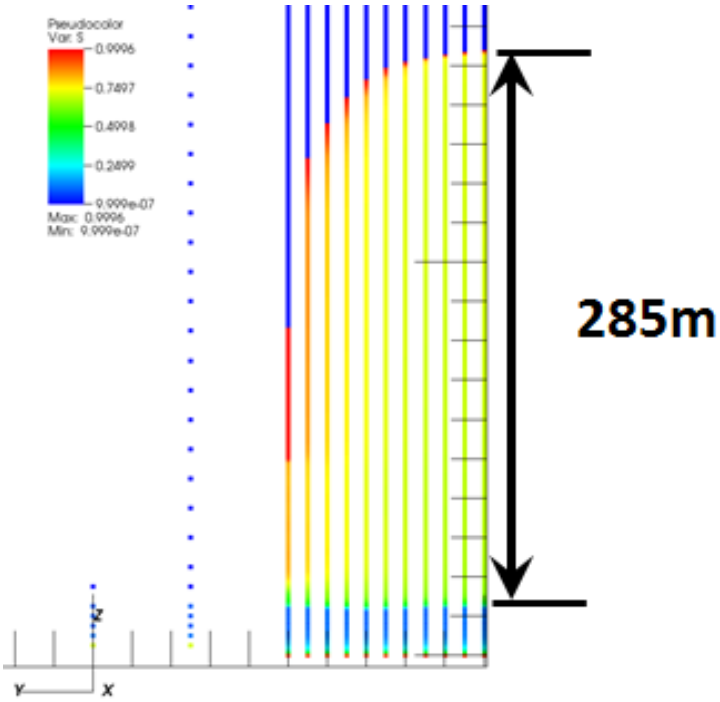

Figure 16 — Gas saturation distribution in the fracture of Problem A4 at t = 255 days, caused by the rising gas plume.